

Evaluation of two GCMs in simulating rainfall inter-annual variability over Southern Africa

Nana Ama Browne Klutse · Babatunde J. Abiodun ·
Bruce C. Hewitson · William J. Gutowski ·
Mark A. Tadross

Received: 9 July 2013 / Accepted: 18 December 2014 / Published online: 11 January 2015
© Springer-Verlag Wien 2015

Abstract We evaluate the performance of two global circulation models (GCMs) over Southern Africa, as part of the efforts to improve the skill of seasonal forecast from a multi-model ensemble system over the region. The two GCMs evaluated in the study are the Community Atmosphere Model version 3 (CAM3) and the Hadley Centre Atmospheric Model version 3 (HadAM3). The study analyzed 30-year climate simulations from the models and compared the results with those from Climate Research Unit (CRU) and National Center for Environmental Prediction (NCEP) reanalysis dataset. The evaluation focused on how well the models simulate circulation features, seasonal variation of temperature and rainfall, and the inter-annual rainfall and circulations during El Niño Southern Oscillation (ENSO) years. The study also investigated the relationship between the regional rainfall from the models and global sea surface temperature (SST) during the El Niño and La Niña years. The results show that both GCMs simulate the circulation features and the seasonal cycles of rainfall and temperature fairly well. The location and magnitude of maxima and minima in surface temperature, sea level pressure (SLP), and rainfall fields are well reproduced. The

maximum error in the simulated temperature fields is about 2 °, 4 mb in SLP and 8 mm/day in rainfall. However, CAM3 shows a major bias in simulating the summer rainfall; it simulates the maximum rainfall along the western part of Southern Africa, instead of the eastern part. The phase of the seasonal cycles is well reproduced, but the amplitude is underestimated over the Western Cape. Both CAM3 and HadAM3 give reasonable simulations of significant relationship between the regional rainfall and SST over the Niño 3.4 region and show that ENSO strongly drives the climate of Southern Africa. Hence, the model simulations could contribute to understanding the climate of the region and improve seasonal forecasts over Southern Africa.

1 Introduction

Seasonal forecasting is an important tool in managing climate risks. Information from seasonal forecasting helps planning and decision making on security-related issues, such as water resource management, disaster prediction and prevention, health planning, and agriculture management. However, seasonal forecast is only useful if it is reliable. As a reliable forecast can help reduce losses from disaster (such as floods, drought, and heat waves), an unreliable forecast can mislead and increase damages from disasters. The reliability of a seasonal forecast over a region depends on how well the climate models used for the forecast can simulate the seasonal and inter-annual variations of dominant climatic features over the region. Hence, to help quantify the reliability of a seasonal forecast system, it is essential to benchmark the ability of the climate models in capturing the dominant climatic features.

In Southern Africa, seasonal forecasting has not achieved the desired skill, especially for agricultural enterprises where a

Electronic supplementary material The online version of this article (doi:10.1007/s00704-014-1356-z) contains supplementary material, which is available to authorized users.

N. A. B. Klutse (✉)
Ghana Space Science and Technology Institute, Ghana Atomic
Energy Commission, Kwabenya, Accra, Ghana
e-mail: amabrowne@gmail.com

B. J. Abiodun · B. C. Hewitson · M. A. Tadross
Climate System Analysis Group, Department of Environmental and
Geographical Science, University of Cape Town, Cape Town, South
Africa

W. J. Gutowski
Department of Geological and Atmospheric Sciences, Iowa State
University, Ames, IA, USA

slight change in predicted weather event could cause losses in crop and livestock production. To address this challenge, several South African institutions (i.e., Climate System Analysis Group (CSAG) and the South African Weather Service, SAWS; and Centre for Scientific and Industrial Research (CSIR)) have harnessed efforts and resources in developing a multi-model forecasting system (Landman et al. 2001a; Landman and Goddard 2002; Klopper and Landman 2003). In the system, seasonal forecasts are obtained by averaging simulations from many global circulation models (GCMs). The philosophy behind this approach is that a forecast from a multi-model ensemble system would be better than the one from a single-model forecast and that the more models used in making a forecast, the better the forecast. However, a caveat with this idea is that adding a new model to a multi-model system may not necessarily improve the skill of the system. If the new model cannot simulate the climatology and seasonal and inter-annual variability of the dominant atmospheric features over the region well, the model results would reduce the skill of the system rather than improve it. Therefore, it is necessary to evaluate the performance of each model participating in a multi-model ensemble forecast system. The evaluation would guide not only in selecting suitable models but also in identifying the strength and weakness of each model and in obtaining appropriate weights to average the model results for the forecast. In addition, the evaluation would help identify atmospheric processes that the models simulate well and those that they fail to simulate. Such information is crucial for model development. Hence, the present study evaluates the performance of two GCMs in simulating the Southern Africa climate and attempts to give reasons for the models' limitations where applicable.

A few studies have evaluated the climate of Southern Africa using GCMs (Engelbrecht et al. 2009; Landman et al. 2001a, b; Landman and Goddard 2002). However, most of these studies either considered a short time period of evaluation (e.g., Landman et al. 2001b; Landman and Goddard 2002; Bartman et al. 2003) or over a smaller area in the region (e.g., Reason et al. 2003) or concentrated on one GCM (e.g., Engelbrecht et al. 2009; Shongwe et al. 2006). The present study reexamines the Southern African climate over a 30-year period (1971–2001) using two GCMs.

Moreover, a number of studies have shown that the climate of Southern Africa is a product of complex interactions between synoptic-scale and meso-scale features, in which topography and sea surface temperature (SST) play a modulating role (e.g., Reason 2002; Tyson and Preston-Whyte 2000). The important circulation features over Southern Africa include the inter-tropical convective zone (ITCZ), the subtropical jets, the high-pressure systems over the South Atlantic and Indian oceans, and the extra-tropical Rossby waves. In the summer, the ITCZ controls the location of maximum moisture flux convergence and maximum rainfall over the region (e.g.,

Newell and Kidson 1984; Kraus 1977; Klaus 1978; Nicholson et al. 1996; Usman and Reason 2004; McGregor and Nieuwolt 1998; Jury and Pathack 1993; Nicholson 2000; Cook 2000; Suzuki 2011). The subtropical jets organize convective storms and induce cyclogenesis (Thorncroft and Flocas 1997; Uccellini and Johnson 1979; Nakamura and Shimo 2004; Roca et al. 2005); at the same time, the jets could produce divergence and stability that hinder rainfall. The Rossby waves (mainly zonal numbers 1 and 3) modulate the strength and motion of storms and other localized features and thus influence rainfall and temperature from these features; for instance, Tyson (1980) linked changes in the position of wave 3 with 10–12-year rainfall oscillation over the south coast of Southern Africa. The anticyclone over the South Indian Ocean produces strong surface pressure gradient between the subcontinent and the Indian Ocean and advects moist unstable air inland to produce strong convection with heavy rainfall and thunderstorms over the eastern part of Southern Africa. Notably, if the anticyclone retreats to the northwest, then southwestern South Africa becomes wetter. Hence, the ability of a GCM in replicating these features could influence the seasonal forecasting skill of the model. In the present study, investigations on how well two GCMs reproduce the circulation features are made.

Rainfall over Southern Africa is generally seasonal. The peak of the rainy season occurs in the summer, from December to February (DJF) with the exception of the Western Cape which is a winter rain area with rainfall occurring mostly from June to August (JJA). Mean summer rainfall contributes most of the mean annual rainfall over Southern Africa. The seasonal rainfall pattern is discussed in several studies including Taljaard (1986) and Harrison (1984). Summer conditions of the southeastern part are often associated with negative sea level pressure (SLP) anomalies over the western Indian Ocean, reducing the northeasterly flux of tropical moisture into the region (Mason and Jury 1997; Rocha and Simmonds 1997). Along the southern and western coasts, winter rainfall results from temperate frontal systems embedded in the westerlies (Tyson and Preston-Whyte 2000).

The spatial and temporal variations of the global SST also influence Southern African climate. In particular, El Niño Southern Oscillation (ENSO) event causes extreme weather conditions such as floods, droughts, and other weather disturbances in many regions of the world (Rasmusson and Wallace 1983; Halpert and Ropelewski 1992). In effect, a quantitative assessment of possible effects of changes in the climate with relation to the ENSO events will provide important information for managing the effects of such changes. As an initial step in estimating possible future changes caused by the ENSO phenomenon from global models, it is necessary to carefully show how the models reproduce the current rainfall variability based on investigation of the atmospheric circulations, which form the main forcing factors for controlling

variability during the El Niño and La Niña years. The present study sheds more light on the models' capability and suitability in simulating the inter-annual variability of rainfall. The impact of SST represented by each model during the summer (winter for Western Cape) of El Niño and La Niña years over different parts of Southern Africa is investigated.

Hence, the aim of this study is to assess the capability of two GCMs in simulating the Southern African climatic features. In this study, the investigation focused on

1. the spatial distribution of temperature and rainfall,
2. the time series of rainfall variability,
3. the circulation features that control the rainfall of the subcontinent, and
4. the influence of global SST on the seasonal rainfall during ENSO years.

The two models used are the Community Atmospheric Model version 3 (CAM3) and the Hadley Centre Atmospheric Model version 3 (HadAM3). A brief description of the GCMs is given in Sect. 2; the section also describes the model experiments, simulation, and analysis in the study. Sections 3–5 present the results and discussions, while Sect. 6 gives the concluding remarks.

2 Model descriptions and simulation

CAM3 is the fifth-generation NCAR atmospheric GCM (Collins et al. 2004). It is the atmospheric component of the fully coupled Community Climate System Model (CCSM). There are three hydrostatic and dynamic cores in CAM3: finite volume (FV), Eulerian spectral (ES), and semi-Lagrangian spectral (SS). For this study, we used an FV dynamic core, which solves the equations for horizontal momentum, potential temperature, pressure thickness, and transport of constituents (including water vapor) using a conservative flux form of the semi-Lagrangian scheme in the horizontal (Lin and Rood 1996) and a Lagrangian scheme with conservative remapping in the vertical. Detailed formulations of other dynamic cores are given in Collins et al. (2004). The physics packages in CAM3 consist of moist (precipitation) processes, cloud and radiation calculations, surface models, and turbulent mixing processes. In the moist processes, CAM3 uses a plume ensemble scheme (Zhang and McFarlane 1995) to parameterize deep convection, a mass flux scheme (Hack 1994) to represent shallow convection, the Sundqvist (1988) scheme for evaporation of convective precipitation as it falls toward the surface, and a prognostic condensate scheme (Rasch and Kristjánsson 1998) combined with a bulk microphysical parameterization scheme (Zhang et al. 2003) to represent non-convective clouds. Collins et al. (2004) gives detailed descriptions of CAM3 physics parameterizations.

HadAM3 is the atmosphere component of the Hadley Centre Coupled Model version 3 (HadCM3). It was developed at the Hadley Centre for Climate Prediction and Research, UK (Gordon et al. 2000; Pope et al. 2000). The model employs spherical polar coordinates on a regular latitude-longitude grid. HadAM3 has resolution of 3.75×2.5 in latitude and longitude. This gives resolution of approximately 300 km, roughly equal to T42 in a spectral model. The convective scheme is Mass Flux scheme (Gregory and Rowntree 1990) with convective downdraughts (Gregory and Allen 1991). The development and description of the HadAM3 model are documented in Gordon et al. (2000), Pope et al. (2000), Jones et al. (2005), and Murphy et al. (2002). HadAM3 is participating in the multi-model forecasting system over Southern Africa.

For this study, we applied both CAM3 and HadAM3 to produce 30-year (1971–2000) climate simulations, forced with the Reynolds' SST (Reynolds 1988). Five-member ensembles are produced from each model by perturbing the initial SST. Ensemble forecasting is one of the best methods for reducing errors associated with climate uncertainties over individual model ensemble prediction. It is envisaged that the greater the number of ensemble members used, the more robust the results, but only five members are used in the study due to our limited computing resources. In the simulations, each model used its default resolution; CAM3 used $2.0^\circ \times 2.5^\circ$ (latitude \times longitude) horizontal resolution and 26 vertical levels; HadAM3 used $3.75^\circ \times 2.5^\circ$ (latitude \times longitude) horizontal resolution and 19 vertical levels.

For the validation, we used the Climate Research Unit (CRU) observational dataset (Mitchell et al. 2004) and the US National Center for Environmental Prediction (NCEP) reanalysis (Kalnay et al. 1996). The resolution of CRU is $0.5^\circ \times 0.5^\circ$ and that of NCEP is $2.5^\circ \times 2.5^\circ$ grid. The simulated winds are validated with NCEP, while the precipitation field is validated from both CRU and NCEP datasets. To validate the ability of the models in simulating mid-latitude waves, we use spectral analysis to obtain the zonal wave numbers 1 and 3 from 500-mb geopotential height in the models and NCEP reanalysis. We compare the simulated and observed long-time mean of surface temperature, pressure, wind vector, quasi-stationary waves, and rainfall for January and July over the domain of interest (Africa and Southern Africa). For the inter-annual variability of rainfall, we computed the annual anomalies in each dataset with respect to long-term mean of the dataset. The agreement between the anomalies for models and that of CRU is quantified with standard deviation, phase synchronization, and correlation analysis. The influence of the SST on the seasonal rainfall is quantified using correlation analysis.

Previous studies have shown that seasonality and inter-annual variability of rainfall vary greatly over Southern Africa. For instance, Engelbrecht et al. (2009) divided the region into six climatic domains; Nicholson divided the region into 10 climatic domains. However, for brevity, the present study used four

domains from the Engelbrecht et al. (2009) division. The four domains are shown in Fig. 1: 10 S/0 and 7 E/30 E for northwestern (NW), 20 S/5 S and 30 E/42 E for northeast (NE), 34 S/27 S and 26 E/33 E for southeast (SE), and 35 S/32 S and 17 E/20 E for Western Cape (WC) domains. Note that NW and NE are located in the tropics, while SE and WC in the mid-latitudes. Furthermore, NW and WC domains have a boundary with the Southeast Atlantic Ocean which gets cold during the cold tongue season of June–September while SE and NE domains with warm the Indian Ocean. Hence, it is of interest to investigate how the models capture the differences in these climatic domains, in particular, the seasonality, inter-annual variability of rainfall, and the influence of SST on the seasonal rainfall. In obtaining the area average over the domains, the data over the adjacent oceans were masked out as much as possible.

3 Spatial distributions

3.1 Temperature and rainfall climatology

A comparison of the simulated and observed fields shows that both GCMs capture the essential features in the temperature

fields (Fig. 2) over Africa in the summer (January) and winter (July). However, in the daily mean temperature over Africa, the models cannot capture the effects of topography on this field. Figure 3 presents the biases between models and NCEP.

In January (Fig. 2), the models replicate the magnitude and location of the observed temperature maxima (over the West African coast, Sudan, and Namibia) and the temperature minima (over Algeria and Uganda). But, they underestimate the Uganda maximum by about 2 °C. HadAM3 underestimates Namibian maximum by 2 °C, while CAM3 does not reproduce it. In July, the models replicate the location of the temperature maxima (over Sahara, Saudi Arabia, and Congo), the terrain-induced low temperature (over South Africa), and the temperature trough (along the eastern half of Southern Africa). But, the magnitude of the simulated maxima is 2 °C lower than that of CRU and NCEP.

The models equally reproduce the summer and winter rainfall distribution well over Africa (Fig. 4). The features that are well simulated include the zone of maximum rainfall (inter-tropical convergence zone (ITCZ)), which lies between 10° S and 20° S in January and between 5° N and 10° N in July, and the subtropical dry zone induced by subsidence arm

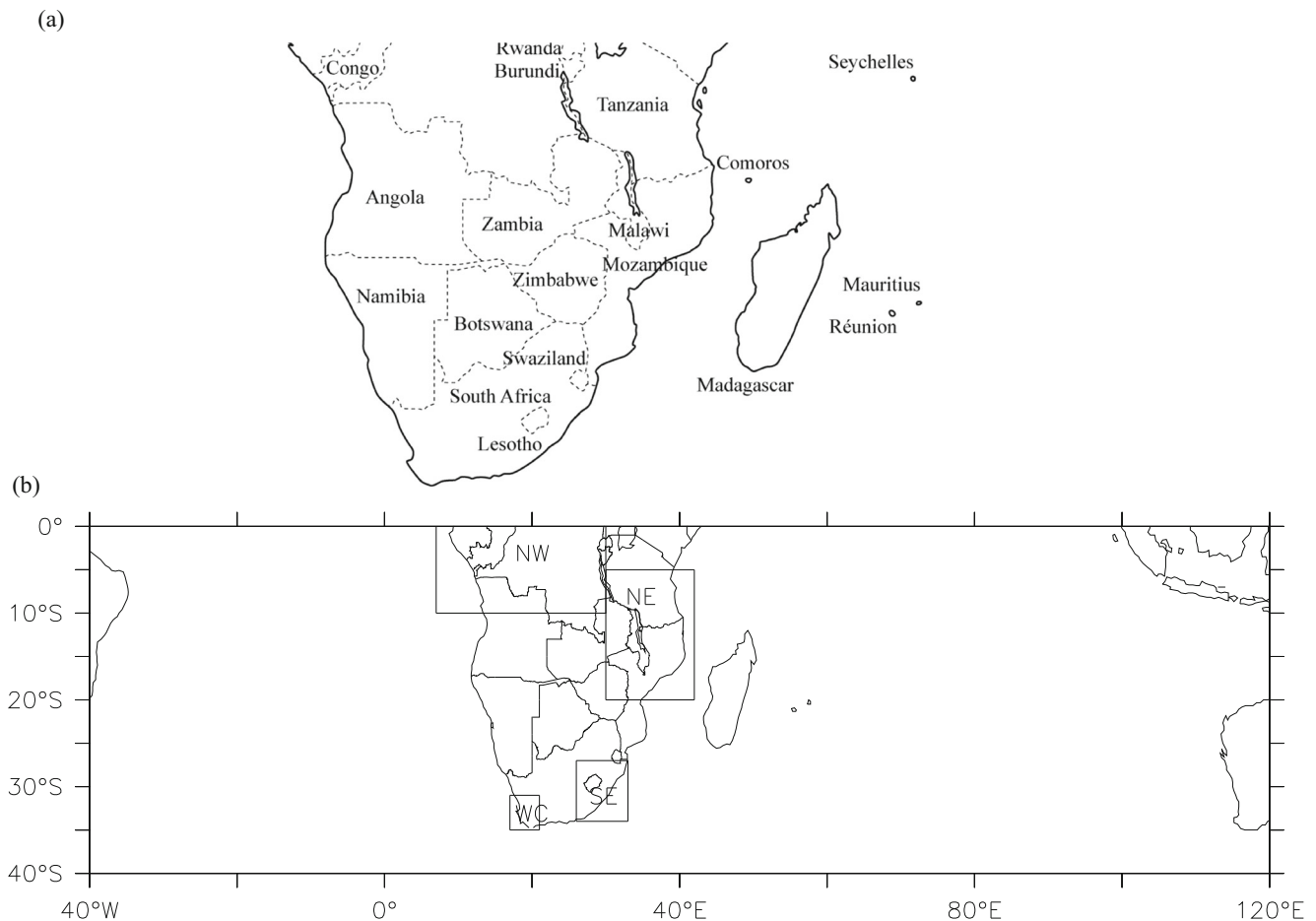


Fig. 1 **a** Geographical map of Southern Africa showing the various countries of the region. **b** The Southern African study domain with the boxed areas showing the locations of the subregions (NW, NE, SE, and WC) used in the study

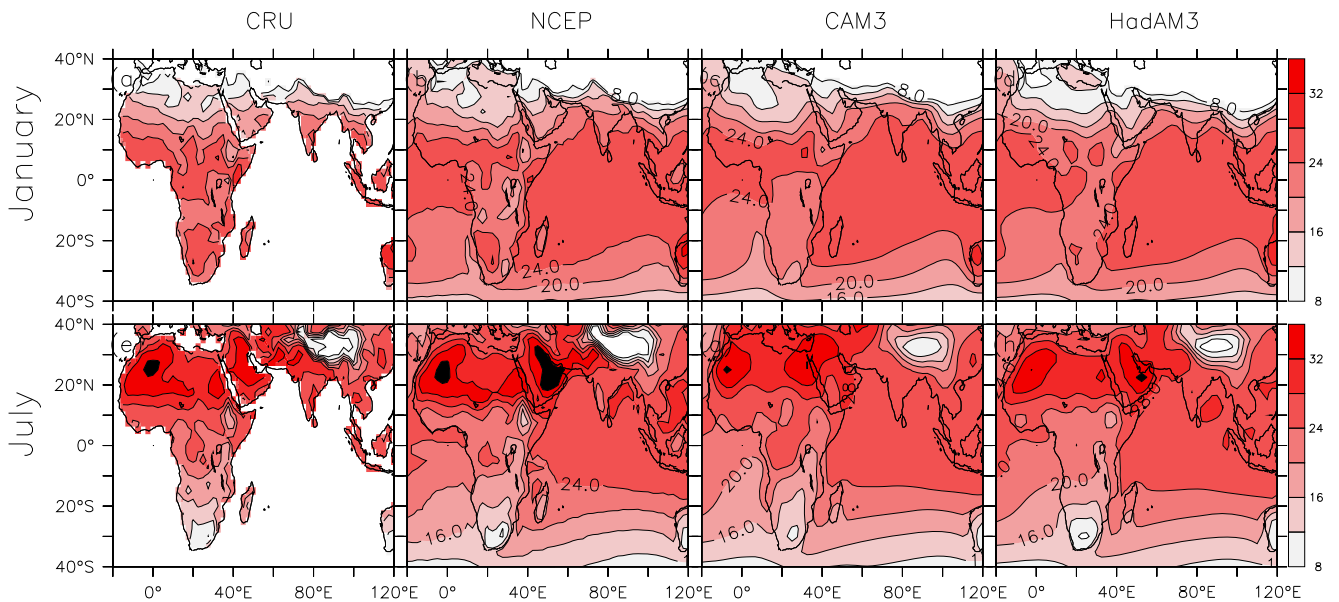


Fig. 2 Comparison of observed and simulated surface temperature (°C) over Africa in January (*upper panels*) and in July (*lower panels*) from CRU, NCEP reanalysis, CAM3, and HadAM3

of Hadley cell. However, there are some disagreements (see Fig. 5) between the simulated and NCEP reanalysis rainfall

patterns. For example, in January, CAM3 displaces the zone of maximum rainfall along the dry western half of Southern

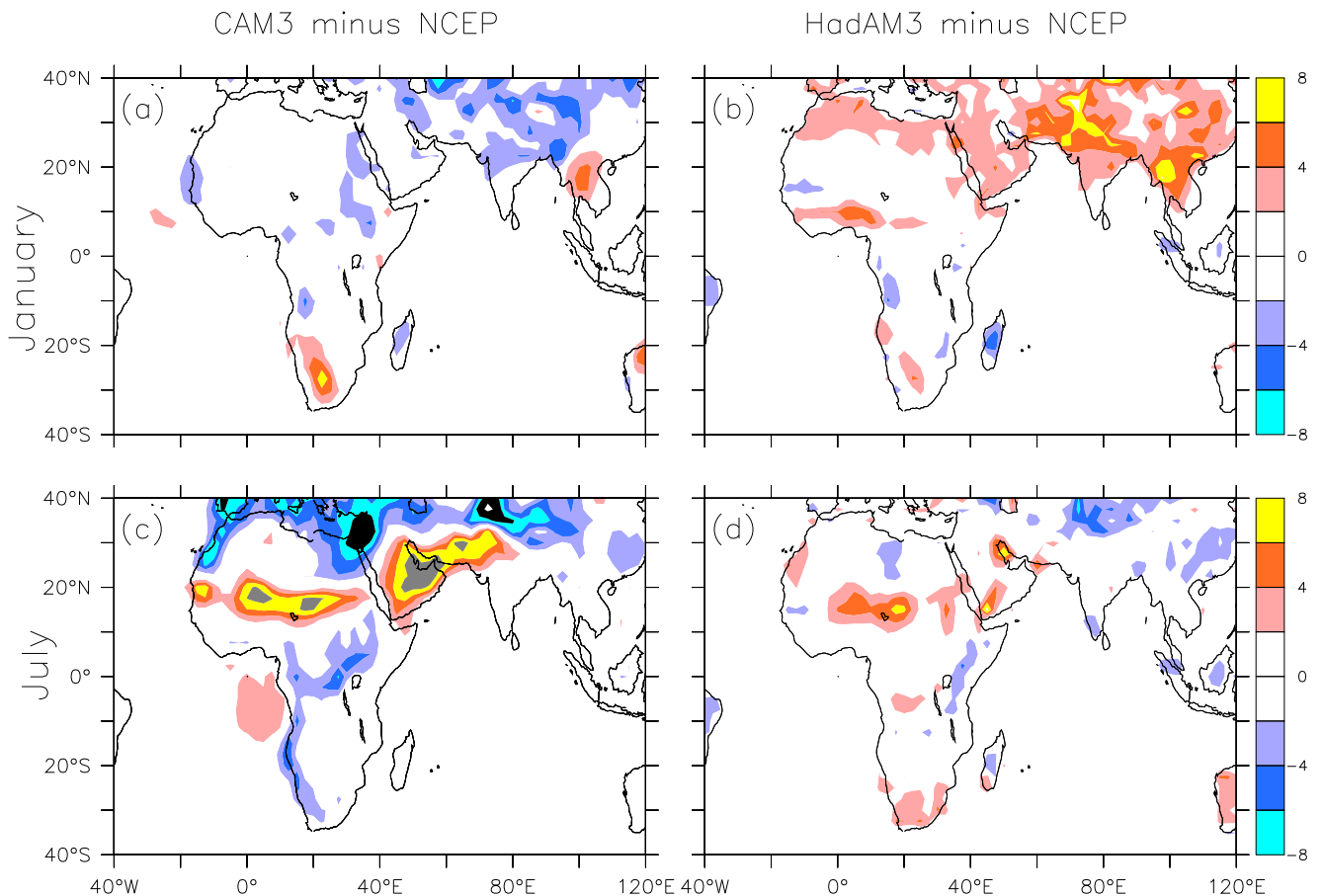


Fig. 3 Differences in temperature (°C) over Africa in January (*upper panels*) and in July (*lower panels*) from CAM3 minus NCEP (*left panels*) and HadAM3 minus NCEP (*right panels*). Biases above 8 °C are shaded in gray and below -8 °C are shaded in black

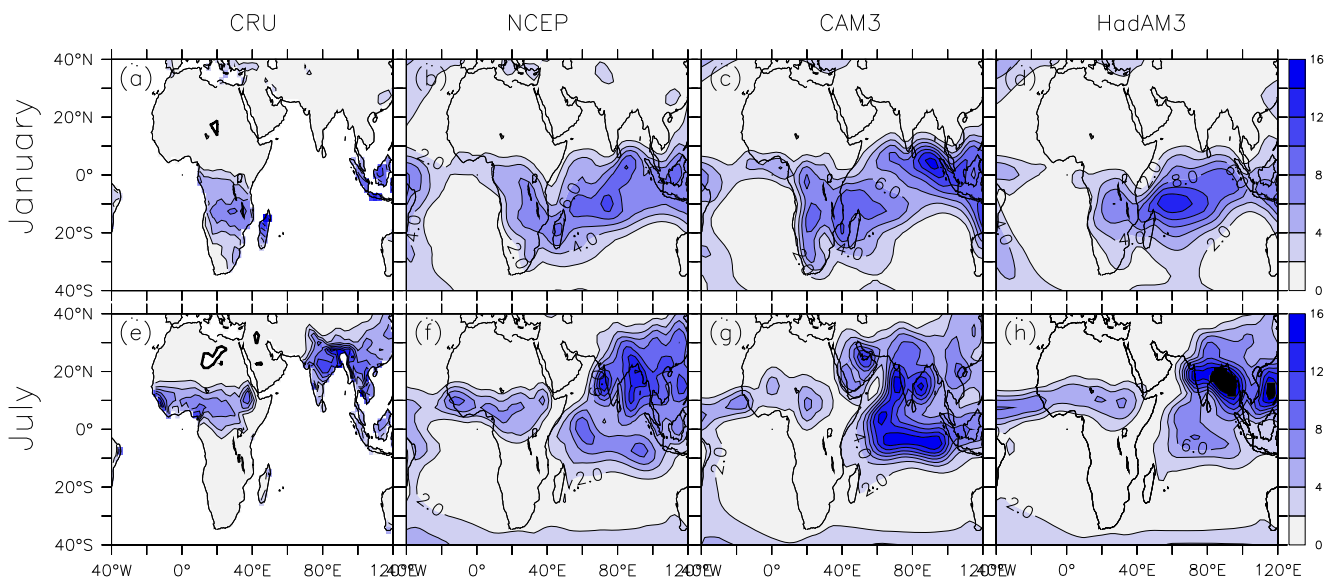


Fig. 4 Comparison of observed and simulated mean rainfall (mm/day) over Africa in January (*upper panels*) and in July (*lower panels*) from CRU, NCEP reanalysis, CAM3, and HadAM3

Africa. In addition, CAM3 significantly overestimates the magnitude of rainfall along the ITCZ in July, whereas HadAM3 captures the pattern but misses the centers of

maxima over the complex terrains probably as an artifact of resolution. Hence, although the models are able to simulate the main features in the spatial distribution of temperature and

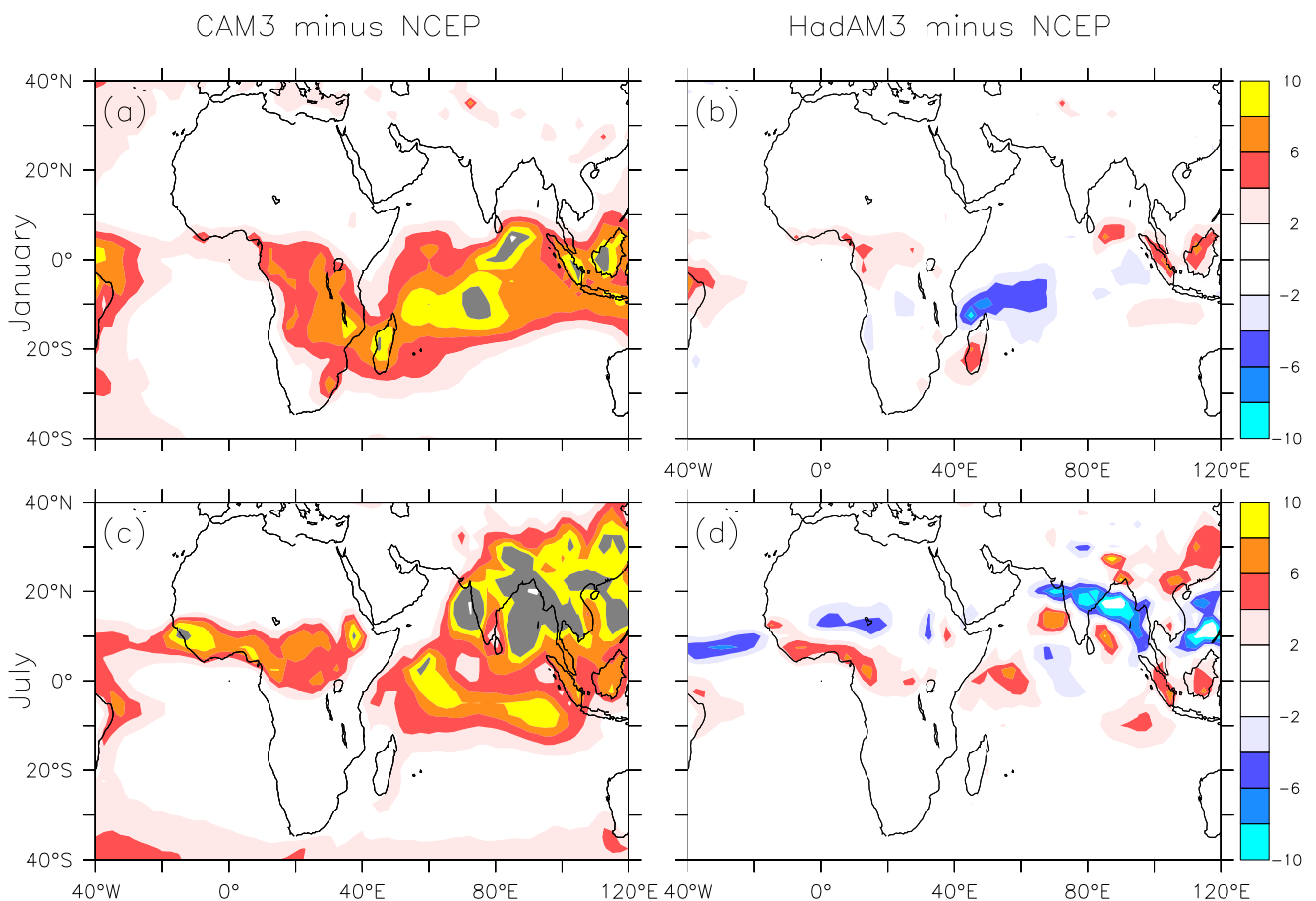


Fig. 5 Differences in rainfall (mm/day) over Africa in January (*upper panels*) and in July (*lower panels*) from CAM3 minus NCEP (*left panels*) and HadAM3 minus NCEP (*right panels*). Biases above 8 mm/day are shaded in gray

rainfall, some biases exist in the magnitude and location of maxima (mostly in CAM3). And, it is thus evident that they have different dynamics in defining rainfall over the region; this should reflect in the circulation patterns.

3.2 Circulation patterns

Although it is established that SST controls seasonal forecasts, understanding how the atmospheric circulation affects seasonal forecasts is a critical step in improving our conceptual understanding of the GCMs. An exploration of why models reproduce the circulation features will inform the quest of reducing uncertainties in a seasonal forecast system. To understand the differences between observation and simulations of circulation features, we discuss here some of the relevant features, including the mean sea level pressure and the wind fields over Africa, the circumpolar waves, and the subtropical jet over Southern Africa.

3.2.1 Climatology of mean sea level pressure and wind

In the pressure and wind fields (Fig. 6), the models capture the locations of the anticyclones with the simulated maximum pressure of about 4 mb higher than observed in January and July. The locations of the

convergence zone over Africa in both seasons are fairly well simulated. The models show that the two trade wind systems converge at the low-pressure zones. However, CAM3 pushes the ITCZ a bit far to the northeast over Saudi Arabia because the southwesterly is too strong over the area, while HadAM3 pushes it to far north over Mali because northeasterlies are weaker over the area. In addition, the effect of temperature on mean sea level pressure distribution is distinct in the model results. Both models show that high pressure weakens over the continent in the winter but is thermally intensified in the summer. This process is more pronounced at the north and south of the continent. However, these circulations do not fully explain the biases in rainfall distribution over Southern Africa in the models; therefore, other circulation features over the region should be important.

3.2.2 Semi-stationary waves

Semi-stationary waves are dominant features of the Southern Hemisphere circulations. It is therefore necessary to see how the GCMs simulate the location and amplitude of Rossby waves with zonal numbers 1 and 3 (hereafter, wave 1 and wave 3, respectively). Wave 1 and wave 3 strongly influence

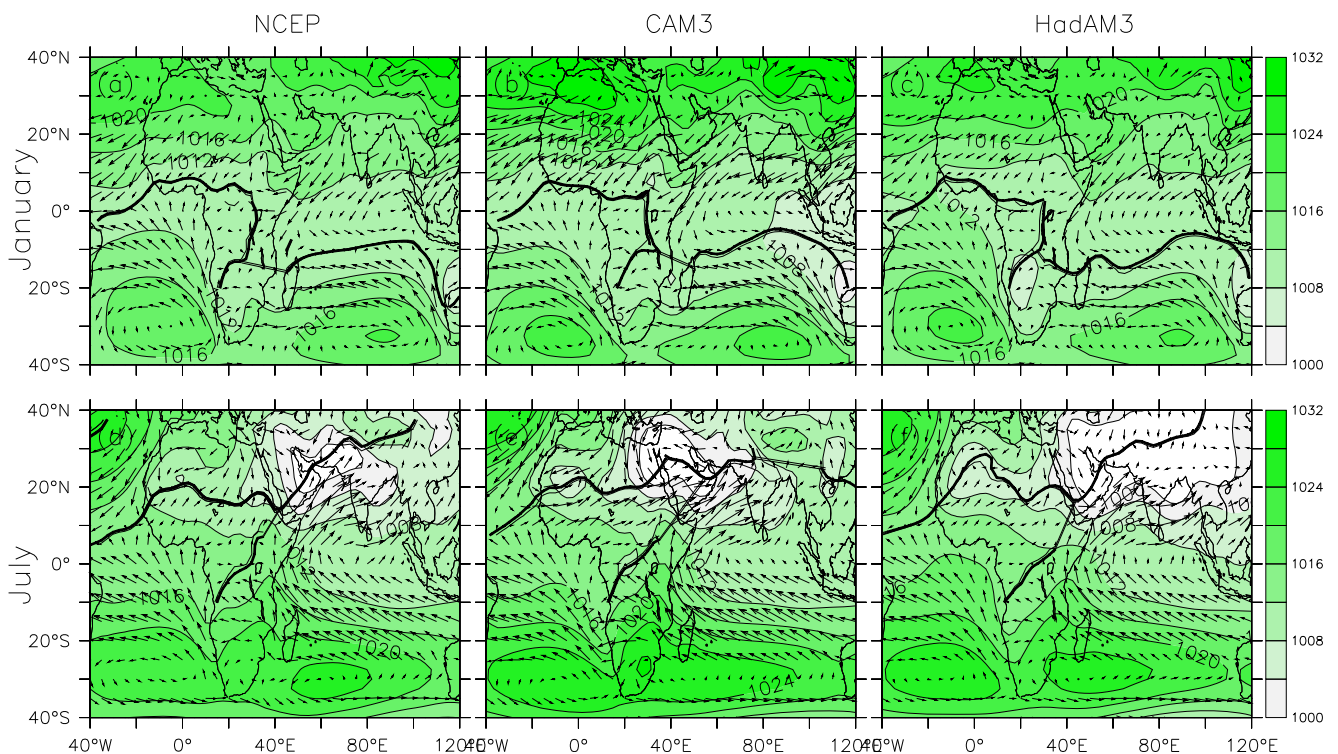


Fig. 6 Comparison of observed and simulated mean sea level pressure distribution (shaded) with wind flow (vectors) over Africa in January (upper panels) and in July (lower panels), from NCEP reanalysis (left

panels), CAM3 (middle panels), and HadAM3 (right panels). In each panel, the arrows show the winds, the lengths of the arrows indicate the wind strengths, and the black bold line demonstrates the path of the ITCZ

the Southern Africa weather and climate (e.g., Mason and Jury 1997; Tyson et al. 1997). The waves are obtained from the 500-mb geopotential height using spectral analysis. For wave 1 (Fig. 7), NCEP reanalysis exhibits a subtropical ridge north of 40° S, and a trough south of it extended toward the high latitudes in both seasons. The magnitudes of these features are more developed in July than in January. The models correctly capture the location of wave 1 ridges and troughs as well as the differences in the magnitudes of the seasons. However, the amplitudes of the wave are generally lower in CAM3 simulation and larger in HadAM3 indicating more subsidence in the latter over the subcontinent, consistent with the rainfall pattern.

Wave 3 (Fig. 8) responds to semi-annual oscillation in the Southern Hemispheric pressure; therefore, the longitudinal position of its peak varies seasonally (Tyson and Preston-Whyte 2000). In January, CAM3 fails to capture the location and orientation of the most prominent troughs and ridges, which have southwest to northeast orientation in the NCEP reanalysis, whereas HadAM3 reproduces these features very well in location, orientation, and magnitude. Similarly in July, HadAM3 simulates more realistic wave pattern as shown in the NCEP. Correct simulation of this wave is critical because it influences substantially the location of blocking anticyclones (Tyson 1981), consistent with the simulated pressure field.

Therefore, comparing this wave pattern to that of rainfall distribution, it is logical that the trough simulated by CAM3 over the southernmost part of the subcontinent along with the weak accompanying ridge might have contributed to the large overestimation of rainfall at the western half of the region.

3.2.3 The subtropical jet

Figure 9 shows the cross section of observed and simulated zonal wind field over Southern Africa. The most prominent feature in the wind field is the subtropical jet, which both GCMs could capture (Fig. 9) but overestimate the strength by 5 m/s. The observed and simulated jet cores shift from 200 mb in January to 100 mb in July. This shift is accompanied by the strengthening and southward displacement of its core away from the subcontinent, making evidence in the more (less) differing temperature in January (July) at the surface (see Fig. 2). When the core of the subtropical jet is over 40–50 S in January, it normally causes air to rise, lowering the air pressure over the area (see Fig. 4) and serving as a source of cloud formation and consequential precipitation and storms.

Comparing the two models, although they simulate the position of the core around the same latitude, the magnitude is much larger in CAM3 indicating more moisture transport (Thorncroft and Flocas 1997; Uccellini and Johnson 1979;

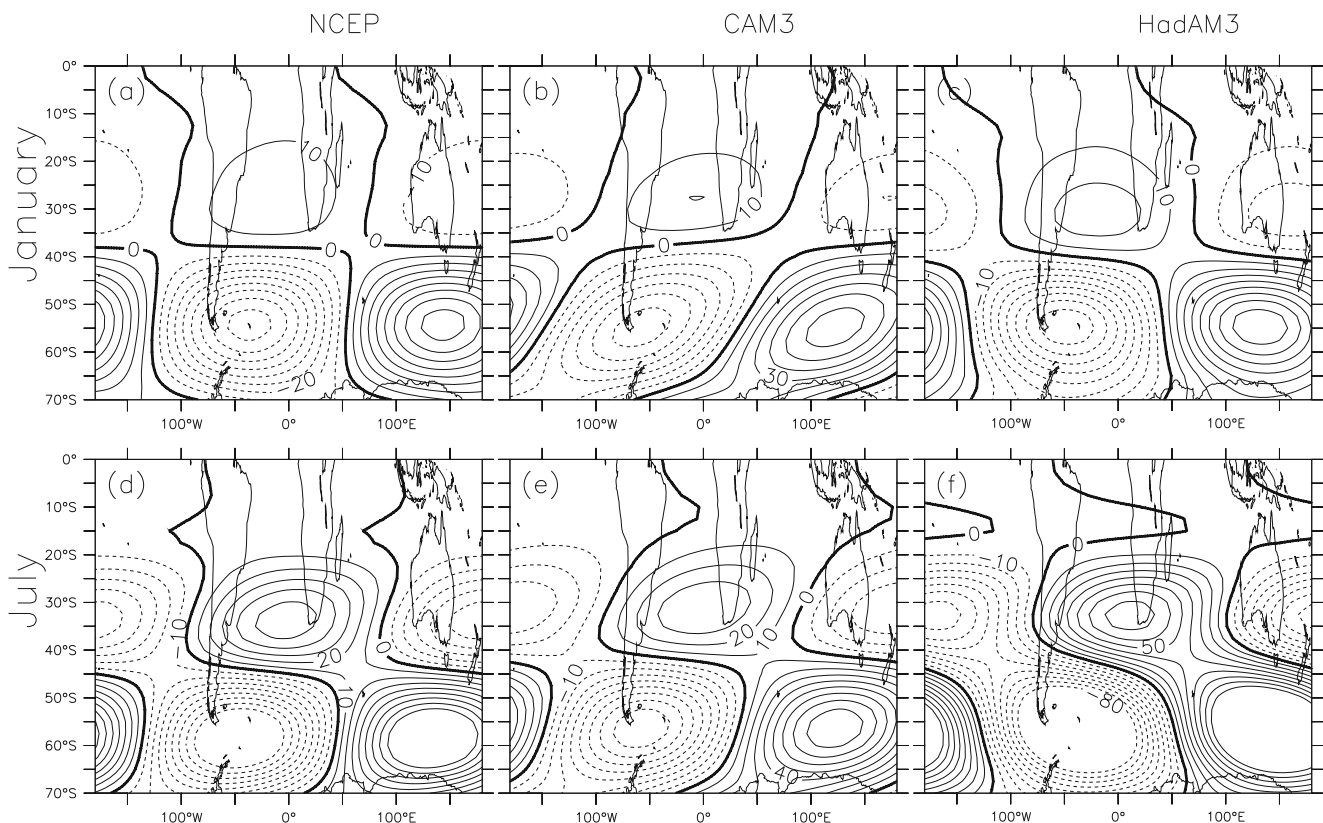


Fig. 7 Comparison of observed and simulated wave 1 over Southern Africa: for January (*upper panels*) and July (*lower panels*), from NCEP reanalysis (*left panels*), CAM3 (*middle panels*), and HadAM3 (*right panels*)

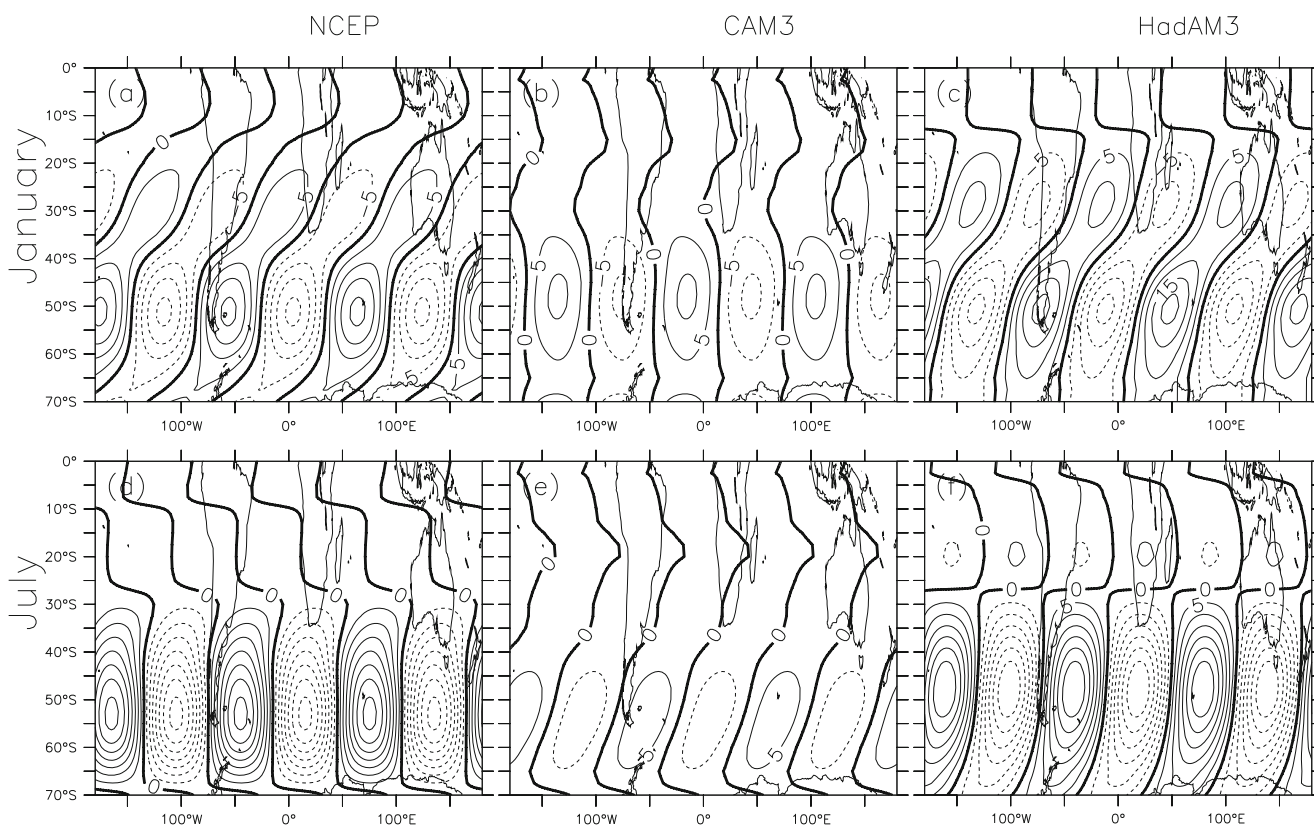


Fig. 8 Same as Fig. 7 but for wave 3

Nakamura and Shimpo 2004; Roca et al. 2005). Other important features which the models also simulate are the low-level and upper level easterlies, although this is not well depicted in HadAM3. However, in January, CAM3 simulates stronger easterlies than NCEP.

4 Temporal variations

4.1 Seasonal variation of temperature and rainfall

In this section, we discuss the capability of the models in reproducing the seasonal variability of annual rainfall and temperature over the four Southern African climatic regions shown in Fig. 1. Figure 10 compares the simulated, NCEP, and CRU daily mean rainfall and temperature patterns over the subregions. The distribution of the mean temperature differs across the four subregions. For instance, CRU shows that, over NW, the maximum temperature (about 25 °C) occurs in February/March and peak rainfall (about 7 mm/day) in November; but over NE, the mean maximum temperature (about 25 °C) is in November, and the peak rainfall (about 7 mm/day) is in February. Over SE and WC, the mean maximum temperature (about 22 and 24 °C, respectively) is in January/February, but the peak rainfall (4.0 and 3.0 mm/day, respectively) is in

February and June, respectively. Over NW, NE, and WC, the minimum temperature occurs in July, but over SE, it is in June. Both models closely reproduced the seasonal patterns of temperature and rainfall over the subregions, with few biases. The main bias is that the simulated minimum temperature is a month late over all the subregions. The maximum error in the simulated temperature is about 2.5 °C (Fig. 10d) for both models. In most cases, CAM3 overestimates the monthly rainfall, while HadAM3 underestimates it, but both models correctly reproduce the seasonal cycle.

4.2 Time series of rainfall

Figure 11 compares the observed, simulated, and NCEP anomalies in the inter-annual DJF rainfall over the four subregions. Only the summer rainfall variability is considered here (except for the WC where the winter rainfall variability is considered) because of its large contribution to the regions' annual rainfall and its connection with synoptic circulation patterns over southern Africa. The anomalies are calculated for 30 years and are expressed in percentage of the mean.

Over the NW, the models agree with both CRU and NCEP in 1972, 1982, 1985, 1994, and 1996. In other years, the models do not agree with either CRU or NCEP. The observed rainfall over NE shows varying anomalies from both NCEP and models. The models are able to capture the rainfall

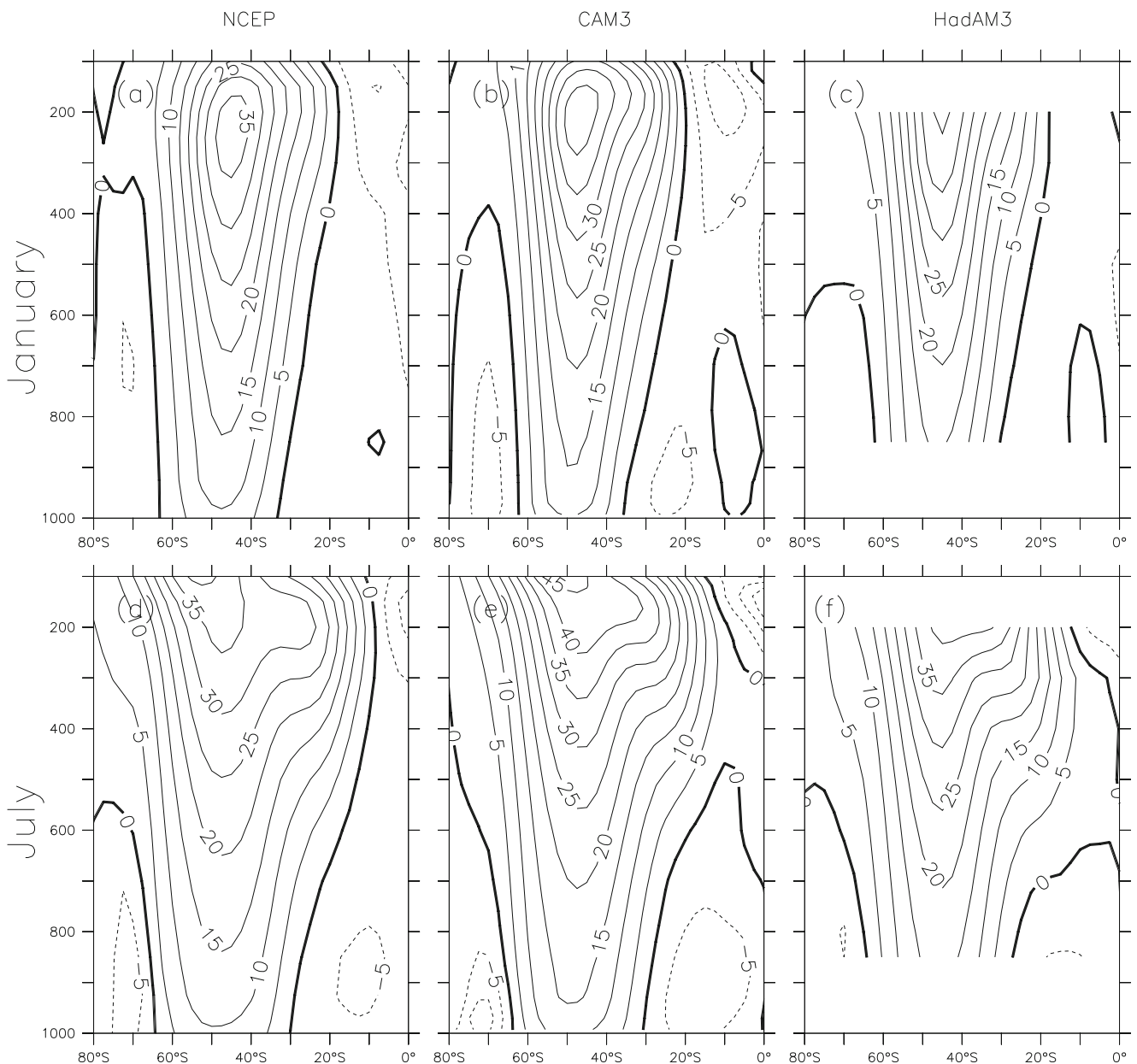


Fig. 9 The vertical structure of zonal wind, average between 20 W and 60 E: for January (*upper panels*) and in July (*lower panels*), from NCEP reanalysis (*left panels*), CAM3 (*middle panels*), and HadAM3 (*right panels*)

patterns in some years well, compared with CRU and NCEP, but disagree in other years with both CRU and NCEP. Apart from 1971, where CRU rainfall over the SE disagrees with the pattern from the models and reanalysis, the models agree more with CRU than with NCEP reanalysis. The models fail to capture the rainfall pattern between 1984 and 1992. The models and NCEP agree with CRU on positive anomalies over WC for 1971, 1974 to 1976, and negative anomaly pattern in 1990 and 1994. The models and NCEP disagree with CRU in 1972, 1973, 1978, and 1986 where they show positive anomaly pattern and CRU shows negative anomaly pattern and in 1993 and 1996 where they show negative anomaly pattern and CRU shows positive anomaly pattern.

NCEP, but not the models, agrees with CRU in negative anomaly pattern in 1979, 1980, 1983, and 1984 and positive anomalies in 1985, 1988, 1989, 1992, and 1995. CAM3 also agrees with CRU for positive anomalies in 1997 and negative anomalies in 1983 and 1984. HadAM3 also agrees with CRU for positive anomalies in 1982 and negative anomalies in 1999. Both CAM3 and HadAM3 but not NCEP agree with CRU for positive anomalies in 1981 and negative anomalies in 1987, 1990, 1997, 1998, and 2000.

Overall, the observation and models largely capture the positive anomaly patterns during the 1982/1983, 1991/1992, 1994/1995, and 1997/98 El Niño periods which brought dry conditions over Southern Africa. The

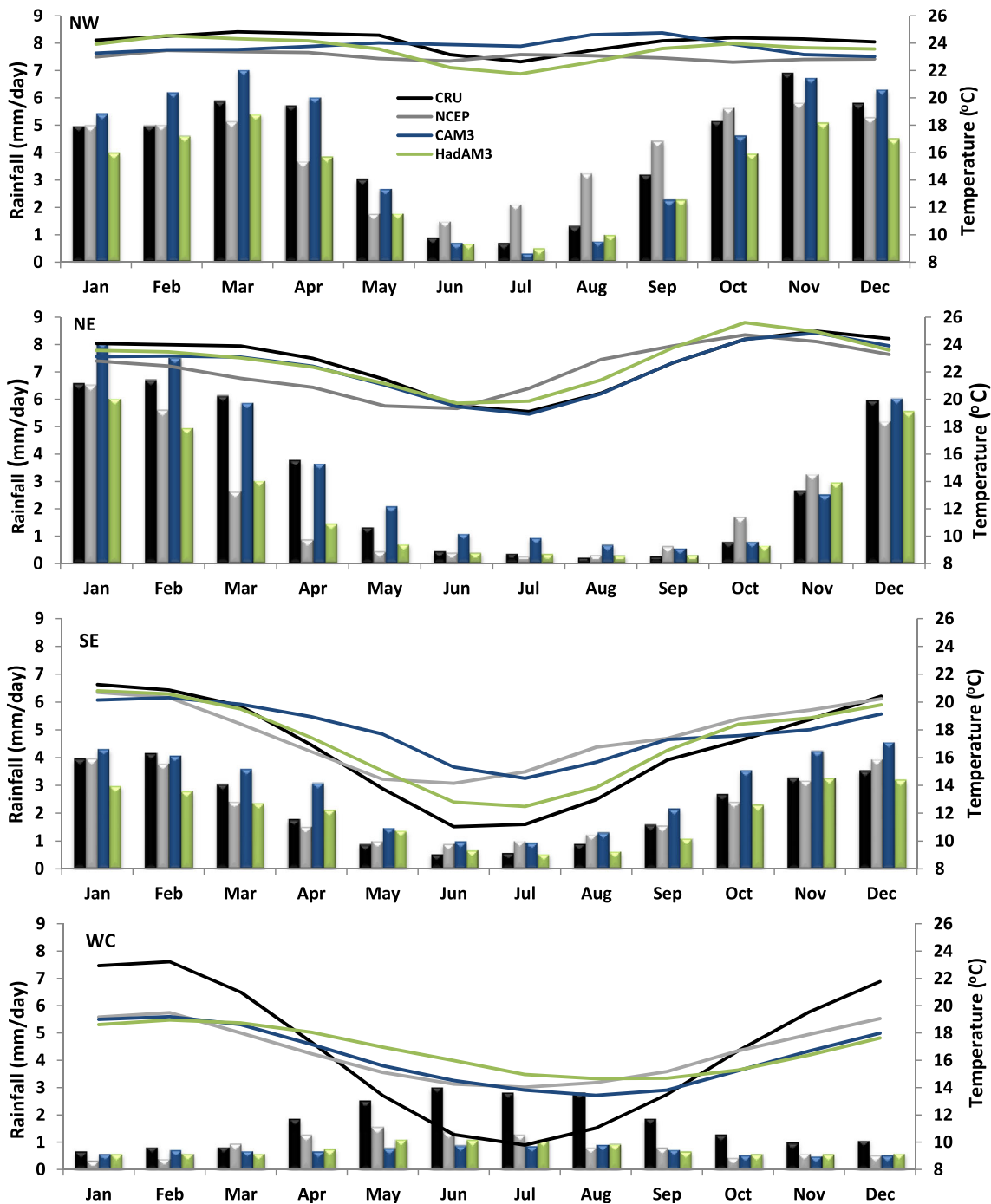


Fig. 10 Monthly variation of simulated and observed mean annual rainfall (bars) and temperature (lines) over different subregions in Southern Africa

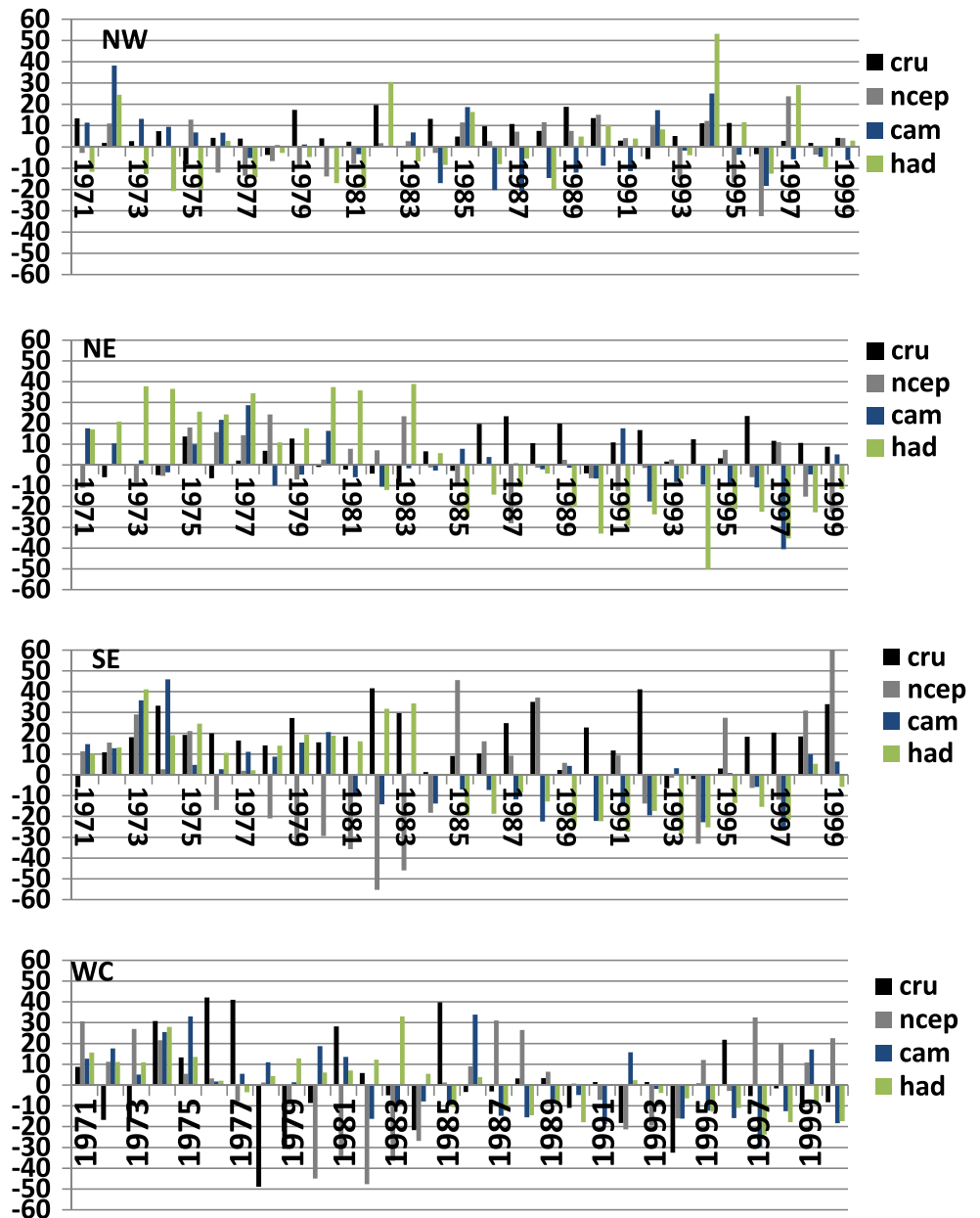
observation and models equally captured the negative anomaly patterns in La Niña years, for example, 1985/1986, 1998/1999, and 1999/2000.

The magnitudes of anomalies from the models (and NCEP) are compared with that from CRU using normalized standard deviation (σ), defined as

$$\sigma = \frac{\sigma_m}{\sigma_c} \tag{1}$$

where σ_m is the standard deviation of the anomalies from the model (or NCEP) and σ_c is standard deviation of anomalies from CRU. The values of σ for models and reanalysis over the four domains are present in Fig. 12 with Taylor diagrams (Taylor 2001). For the models, the standard deviation of the anomalies is close to that of CRU over NE and SE, but higher in NW and lower in WC. NCEP gives a normalized standard deviation of 1.3 and 0.7 over NE and WC, respectively, but about 2 over NW and SE. The spatial standard deviation (not

Fig. 11 Anomalies showing inter-annual variations in DJF rainfall (%) over the subregions (JJA for WC) in Southern Africa

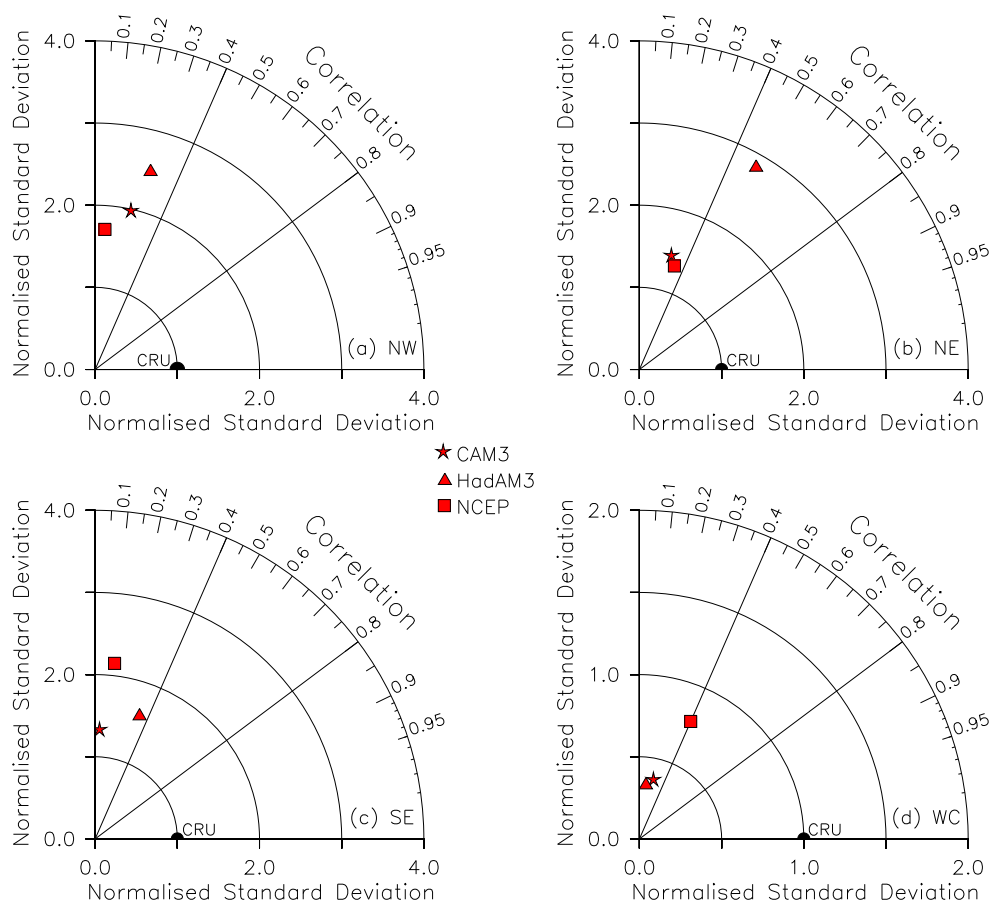


shown) gives the basis for comparing the spatial distribution of the standard deviation from the models, NCEP, and CRU. The spread of standard deviation varies among the models, NCEP, and CRU. CRU has deviations up to 2.5 mm/day over Southern Africa, and the maximum is found at where NE is located. NCEP has deviations up to 1.4 mm/day, and CAM3 has deviations of up to 2.5 mm/day with the maximum over the eastern part of the continent where SE is located, while HadAM3 has up to 3 mm/day deviation at the northern part of the continent where NW is located and 2.5 mm/day over the southeastern part of the continent where SE is located.

The values of correlation coefficients (R), also used to further quantify the agreement of the rainfall anomalies from the GCMs (and NCEP) and those from CRU, are in Fig. 12

from Taylor diagrams (Taylor 2001). In general, the correlation between the model and CRU anomalies is weak. For CAM3, the highest correlation coefficient ($R=0.30$) occurs over NE and the lowest ($R=0.04$) over SE. For HadAM3, the highest correlation coefficient ($R=0.50$) occurs over NE and the lowest over WC ($R=0.05$). For the NCEP, the correlation coefficients are also weak ($R<0.5$), even lower than those for the models in all the domains except over WC. For instance, over NW, the correlation for NCEP is lower than those for both models. This raises the question on the confidence of using reanalysis data for model evaluation over Southern Africa. Several studies have shown similar concern and evaluated rainfall over different parts of the world comparing reanalysis with station or CRU datasets. But, the

Fig. 12 Comparison of NCEP (square), CAM3 (star), and HadAM3 (triangle) with CRU in simulating the DJF rainfall over NW, NE, SE, and JJA rainfall over WC with a Taylor diagram (Taylor 2001)



results that they obtained vary. For example, Rao et al. (2002) demonstrated that the NCEP rainfall data agree well with observational data in some regions of Brazil, while in other regions, the agreement is poor. Similar conclusions were derived from the studies of Yang et al. (1999), Hines et al. (2000), Smith et al. (2001), Rusticucci and Kousky (2002), and Flocas et al. (2004). These studies suggested that parameterization of physical process is what limits the skill of both GCMs and reanalysis data in reproducing rainfall as observed.

The agreement between the rainfall anomalies from the models (and NCEP) and CRU is also quantified in terms of phase synchronization (η ; Misra 1991), defined as

$$\eta = \frac{n-n'}{n} \times 100 \tag{2}$$

where n is the total number of events (30) and n' is the number of cases for which the anomalies have opposite signs (out of phase) with that of CRU. Therefore, η is equal to zero if all the anomalies are out of phase with their CRU counterparts, while $\eta=100$ when all of them are in phase with their CRU counterparts. The values of η for the four domains from the models and reanalysis are given in Table 1.

For the models, the phase synchronization (Table 1) is high over SE and WC ($\eta > 50\%$) indicating that the models are able to capture the occurrences of individual anomalies most of the time with respect to CRU observations. Over the tropical subregions (NE, NW) where η is lower or equal to 50%, the models fail to represent the proper sign of most of the specific events. More specifically, CAM3 represents 40, 43.3, and 53.3%, while HadCM3 represents 50, 33.3, and 56.7% for NW, NE, and SE, respectively. Both models show 63.3% for WC. The phase synchronization of NCEP is 56.7% for all subregions (except over NE, which has 46.7%).

Table 1 Phase synchronization

η (%)	NCEP	CAM3	HadAM3
NW	56.7	40.0	50.0
NE	46.7	43.3	33.3
SE	56.7	53.3	56.7
WC	56.7	63.3	63.3

5 ENSO modulation of summer rainfall

The following results give the composite of the differences between the DJF El Niño/La Niña fields and climatology fields. All anomaly fields are deviations from 30-year (1971–2000) DJF average. The observed fields are computed from CRU (only for rainfall) and NCEP reanalysis dataset, and the corresponding simulated fields are from the ensemble mean of the models simulations. Table 2 shows the ENSO years used in the study.

5.1 Anomalies of rainfall

Figure 13 depicts the dry anomalies during El Niño and wet anomalies during La Niña years. NCEP significantly captures drought in El Niño and large intense rainfall in La Niña years over the eastern part of Southern Africa, which agrees with previous studies (Ropelewski and Halpert 1987; Philander 1990; Ogallo 1994; Reason and Jagadheesha 2005) of the regional impacts of El Niño on weather and climate in boreal winter (astral summer). The models are able to get the basic structure of the ENSO phenomenon in most parts of Southern Africa, especially in the La Niña composite.

5.2 Anomalies of mean sea level pressure

The examination of the composite mean SLP field exhibits high positive anomalies in the El Niño than in the La Niña. In the El Niño composite, positive pressure anomalies are more pronounced especially over the South Atlantic Ocean, in contrast to the La Niña composite in which the negative anomalies are much lower. This demonstrates that the intensified activity over the oceans has a considerable effect on the rainfall during these years. A closer study exposes an additional difference between the composites, this time over Southern Africa (Fig. 14).

The western half of the region experiences higher positive pressure anomalies than the eastern half with lower positive pressure anomalies in El Niño years. Negative anomalies are only in the Indian Ocean in El Niño. In the La Niña composite, high negative values are everywhere over the region with more negative anomalies lower than -20 (shown with gray shades in Fig. 14) over the northern and western part of the region and over the South Atlantic Ocean. Both models reproduce this pattern only to some

Table 2 Years representing specific El Niño and La Niña period from 1971 to 2000 considered in the study

El Niño	1972/1973, 1976/1977, 1977/1978, 1982/1983, 1986/1987, 1987/1988, 1991/1992, 1994/1995, 1997/1998
La Niña	1971/1972, 1973/1974, 1974/1975, 1975/1976, 1985/1986, 1988/1989, 1998/1999, 1999/2000

extent. For instance, CAM3 shows high positive anomalies everywhere over the region in El Niño and high negative anomalies everywhere over the region in La Niña. Similarly, HadAM3 shows the negative anomalies emerging from the Indian Ocean and the positive anomalies from the South Atlantic Ocean, but it fails to simulate the negative anomalies over Madagascar as in NCEP in El Niño but captures the pattern well in La Niña.

5.3 Anomalies of 500-hPa geopotential height

While in the previous section, the El Niño and La Niña impact on rainfall is diagnosed in terms of surface perturbation and since our main interest is on rainfall, which originates essentially in the mid-troposphere, we here examine the composite map of the 500-mb geopotential height (Fig. 15). The 500-mb anomaly composites in El Niño years point to positive geopotential height anomalies over most parts of the region from NCEP, which indicate more subsidence and therefore less rainfall as shown above. In the El Niño anomalies, higher than normal geopotential heights with values between 0 and 4 m are produced over Southern Africa. This is associated with anomalous easterly flow over the northeastern part of the region and a suppression of tropical air masses and subsequent rainfall.

In both models, positive anomalies of geopotential height are more marked over the southern part of the region, which extends to the north in HadAM3. Furthermore, the lower than normal 500-mb heights over the northern part of the region did not extend to the south of the region, resulting in typical rather than especially wet events that seem to play an important role in the pattern of rainfall during La Niña years. Both models display the negative pattern over the region. For example, CAM3 has zero to low negative anomalies in La Niña years, while HadAM3 has a high negative over the south central part of the region, consistent with the rainfall anomalies.

5.4 The role of SST

To assess how the models simulate the relationship between Southern Africa rainfall and SST, the distribution of inter-annual temporal correlation coefficients between DJF (JJA for Western Cape) mean rainfall and DJF mean SST during the El Niño and La Niña years is shown with Figs. 16, 17, 18 and 19 for different subregions of Southern Africa.

In the NW correlation field (Fig. 16), CRU disagrees with NCEP on how well the seasonal rainfall over the region correlates with the SST but shows some agreements with respect to the models. Particularly for the El Niño composite, the positive correlation in the oceans around Africa shown in CRU is not present in NCEP reanalysis and CAM3. HadAM3 shows this correlation, but with lower values. While CRU suggests significant positive correlations over the South Atlantic Ocean and

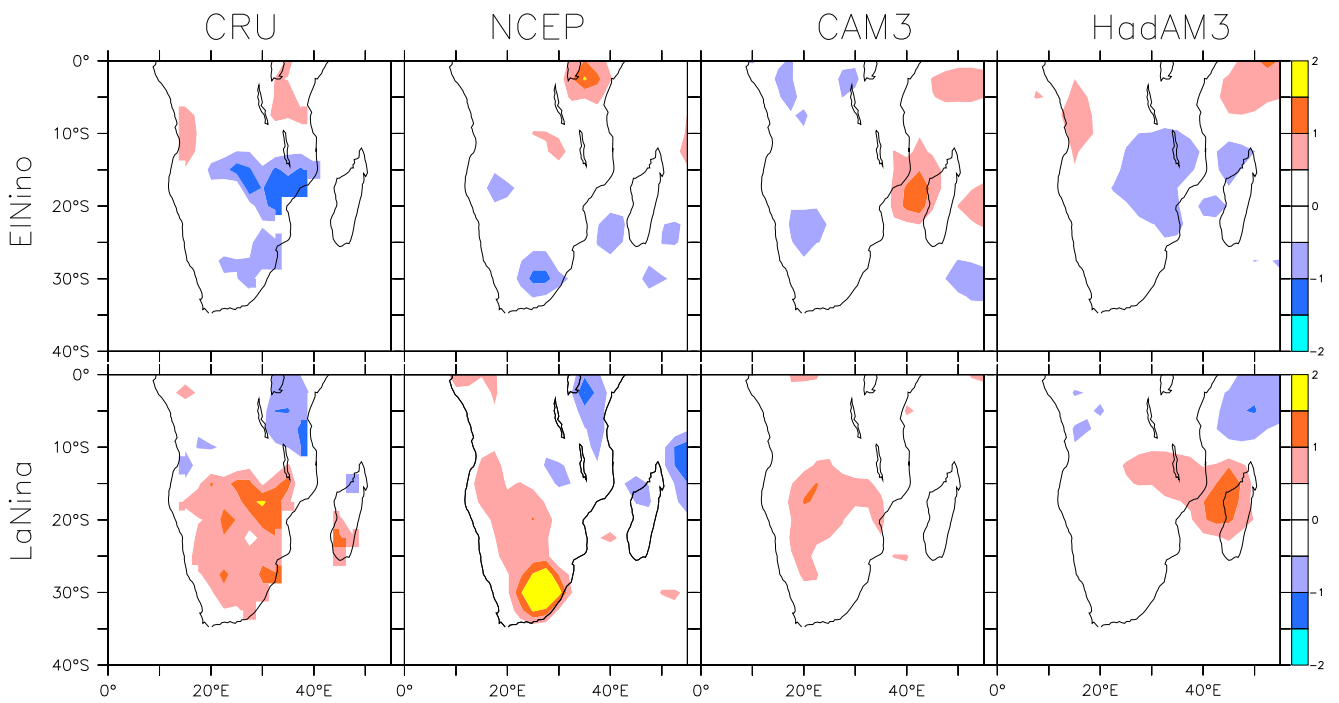


Fig. 13 Comparison of simulated (CAM3 and HadAM3) ENSO years minus mean climatology composite DJF rainfall with CRU and NCEP reanalysis

over the South Indian Ocean, NCEP reanalysis shows contrasting negative correlation patterns. Both models show comparable correlation patterns as CRU. For

instance, both show that the seasonal rainfall over the region has a significant negative correlation ($r > 0.4$) pattern over the Indian Ocean and North Pacific and

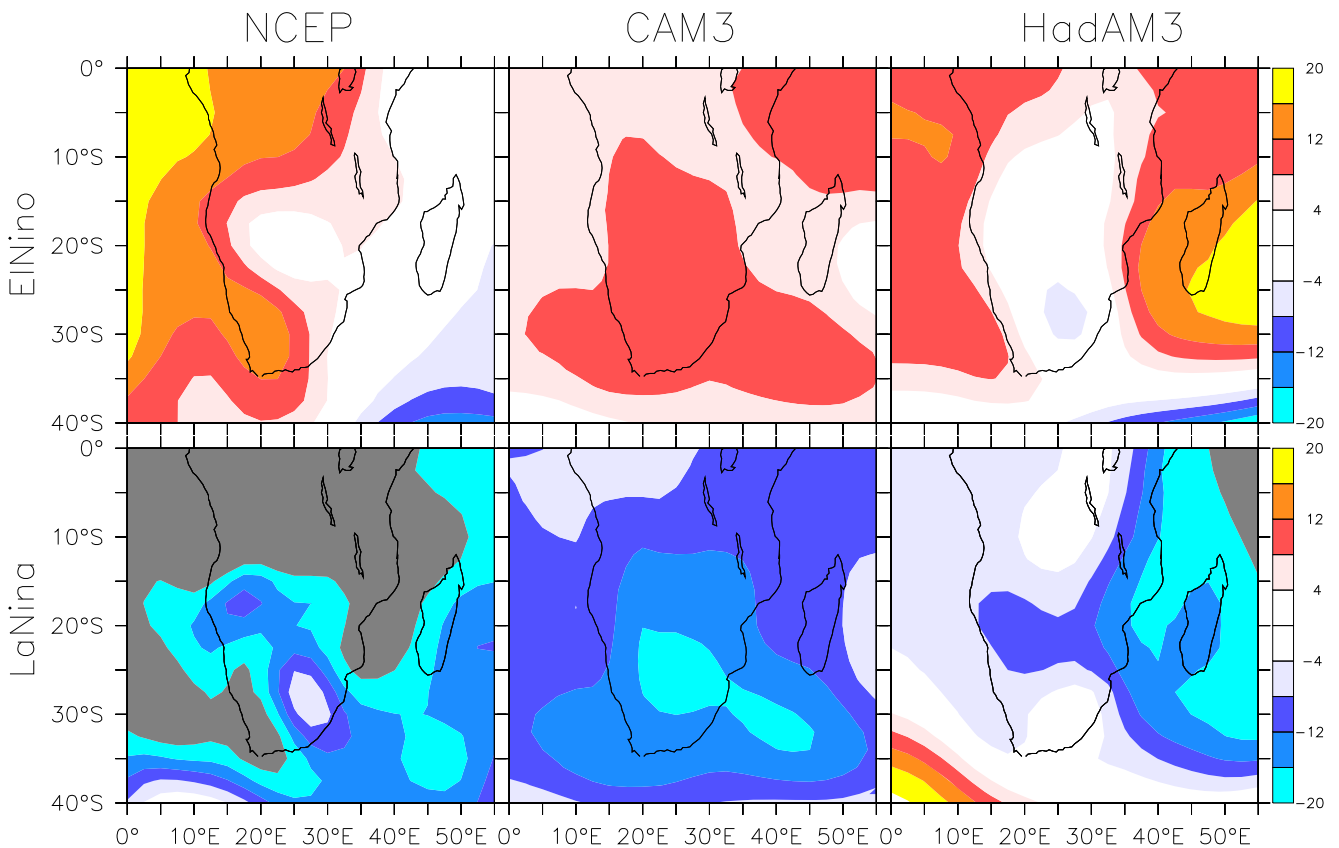


Fig. 14 Comparison of simulated (CAM3 and HadAM3) ENSO years minus mean climatology composite DJF mean sea level pressure with NCEP reanalysis. Values lower than -20 are shaded gray

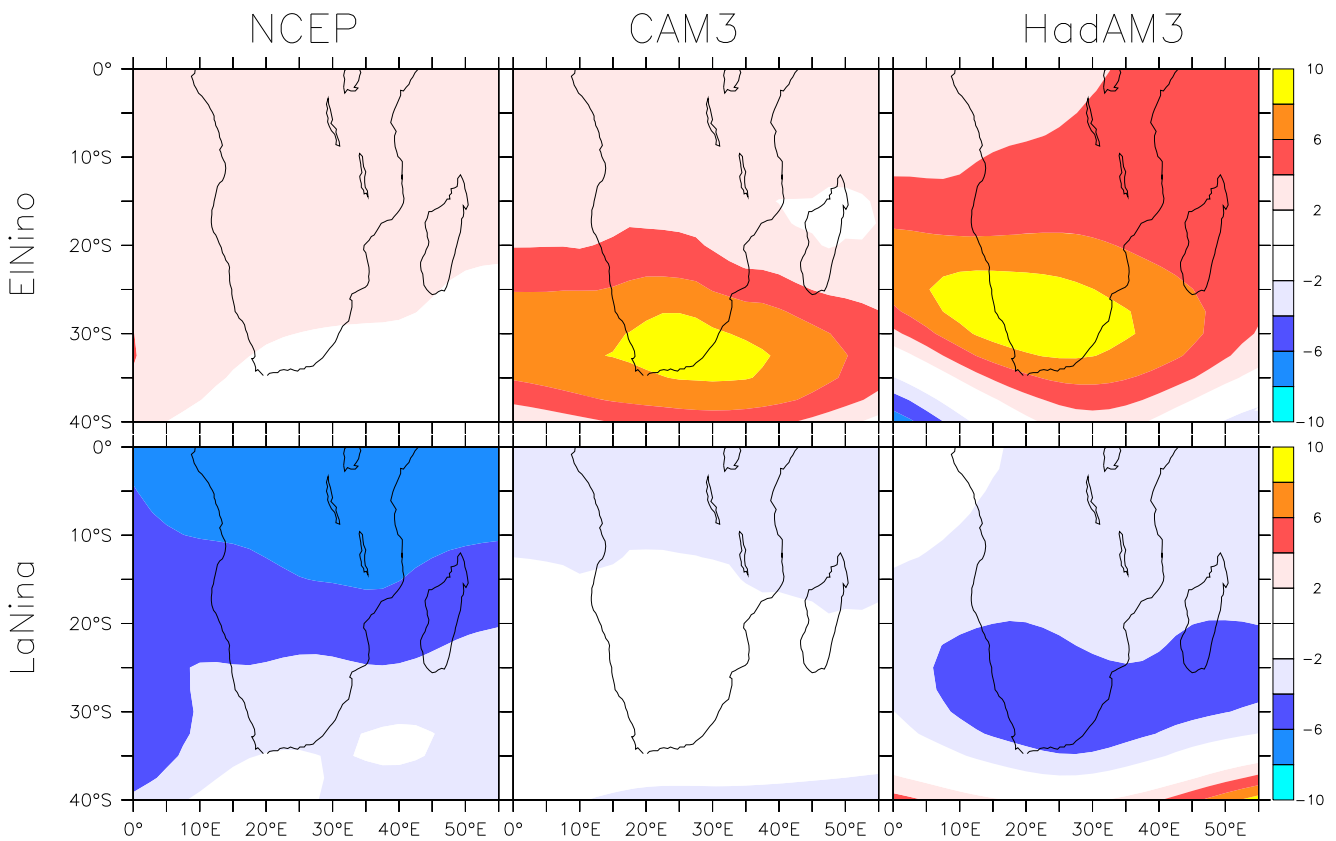


Fig. 15 Comparison of simulated (CAM3 and HadAM3) ENSO years minus mean climatology composite DJF geopotential height at 500 mb with NCEP reanalysis

South Pacific Oceans. On the other hand, in the La Niña composite, CRU shows low correlation coefficients over all the oceans. In addition, no significant correlations are found in the South Atlantic Ocean as in the case of El Niño, but positive correlations are significant in the South Indian Ocean. The models agree more with NCEP than with CRU although they simulate the dipole at the North Pacific Ocean as shown in CRU. In both NCEP and the models, negative correlation values are found everywhere except in a small area in the South Atlantic Ocean near South America and in the North Pacific Ocean.

The rainfall-SST correlation field for NE (Fig. 17) shows disagreements among the models, CRU, and NCEP in both El Niño and La Niña composites. Although CRU shows less significant correlation coefficients over the oceans, NCEP and the models show various degrees of significant correlations. CAM3 agrees with CRU for the correlation over the South Indian Ocean in El Niño and both models in La Niña. In addition, the models show that the seasonal rainfall is negatively correlated ($r = -0.4$, significant at 90 %) with SST over the Pacific Ocean and the Indian Ocean in both composites.

In the rainfall-SST correlation fields for SE, there is a good agreement between the models and CRU to some extent but not with NCEP (Fig. 18). In general, the models suggest a

negative correlation between the rainfall over this region and SST over the Pacific Ocean in both composites. The models also suggest a negative correlation between the regional rainfall and SST over the North Atlantic Ocean, in both composites which disagree with CRU. However, the correlation pattern of NCEP agrees with CRU over the Indian Ocean in only El Niño. NCEP shows a positive correlation with SST over the South Atlantic Ocean and Indian Ocean in El Niño and a negative correlation with the North Pacific Ocean in La Niña.

The rainfall-SST correlation field for WC is done for JJA as the region receives most of its rainfall in that season (see Fig. 10d). In Fig. 19, CRU shows weak correlation with SST over most oceans during El Niño. It shows a strong positive significant correlation at the North Pacific Ocean and south of the Indian Ocean, while a strong negative correlation is found in the South Atlantic Ocean. NCEP shows a negative correlation in the oceans except for the South Pacific Ocean and South Indian Ocean. HadAM3 shows a similar correlation pattern, but CAM3 only shows mostly negative strong significant correlation in the oceans. The correlation during La Niña from CRU and the models shows mostly significant strong negative values between 0.6 and 0.8. CRU shows a strong significant correlation over a small region in the Niño 3.4 regions. This

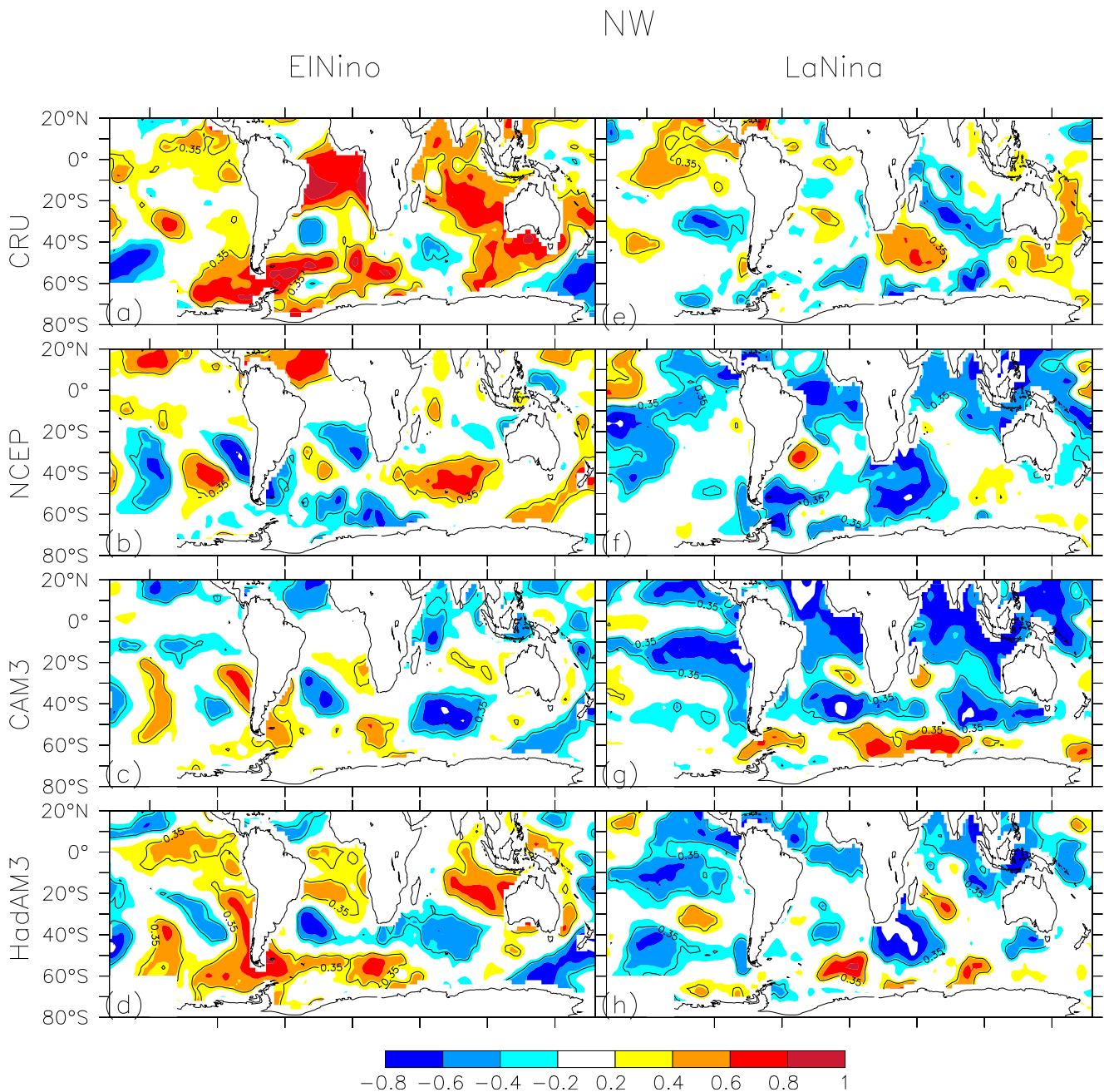


Fig. 16 Distribution of inter-annual temporal correlation coefficients between DJF mean rainfall over the NW subregion and DJF mean global SST for ENSO years from observed, simulated, and reanalysis. Significant values ($r > 0.37$) are in enclosed contours

correlation coefficient is more pronounced in NCEP for most areas.

The disagreement between observation and the reanalysis here shows how difficult it is to link the summer rainfall over the subregions with global SST. This could be because, in observation, there are other smaller scale circulations that control connection between the SST and the seasonal rainfall over the region, but in the reanalysis and models, those smaller scale features may not be fully resolved. The degree to which those smaller scales are resolved depends on the physics parameterizations in the GCMs and the reanalysis.

6 Conclusion

In this paper, we evaluated the performance of two global models (CAM3 and HadAM3) used for seasonal forecasts, in simulating the Southern African general circulation features that control rainfall over the region. Information from the evaluation provides a basis for understanding how well GCMs reproduce climate variability which will thus inform the generation of better seasonal forecasts. To do this, we compared the model simulations for 30 years (1971 to 2000) over Southern Africa with NCEP.

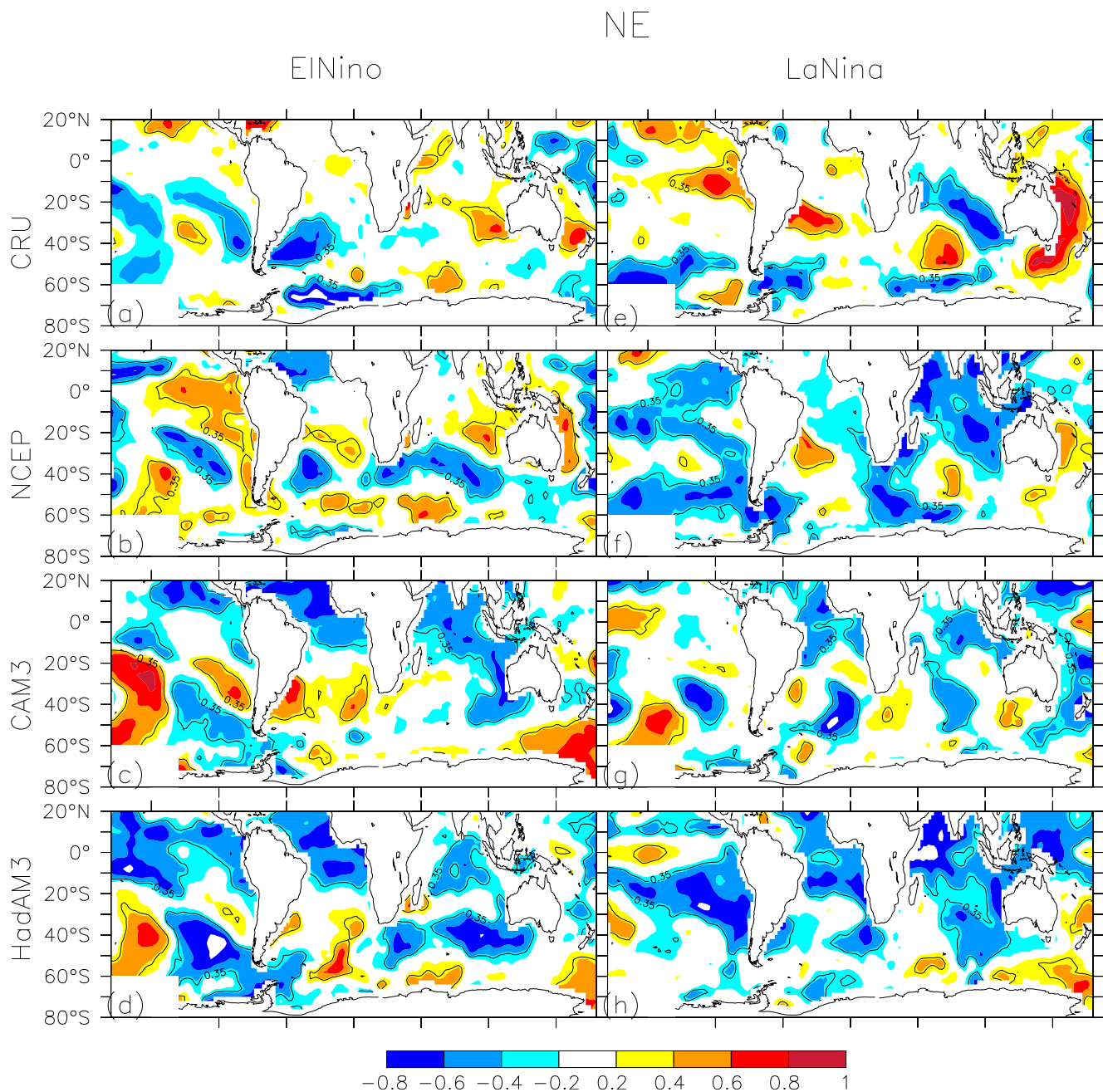


Fig. 17 Same as Fig. 16 but for NE

The results showed that both models reproduce the climate features over Southern Africa but with some biases. In particular, they capture rainfall and temperature spatial distributions, the wind systems, the ITCZ location, subtropical jet, subtropical anticyclones, and wave systems. The main error in CAM3-simulated rainfall distribution is that, in the summer, the maximum rainfall zone is located at the west instead of the east as in the observed and HadAM3 rainfall. HadAM3 shows underestimation of rainfall over the entire domain. For both models, the errors in simulating the temperature field were within 3 °C. For the circulation features, CAM3 performs well

in representing the winds (speed and direction) and the location of ITCZ, while HadAM3 performs better in simulating the circumpolar waves over the region. We explain the overestimation of rainfall over the western part of the subcontinent in CAM3 with its limitation in reproducing the proper location and magnitude of the observed trough of wave 3. The underestimation of rainfall shown in HadAM3 simulation over the region may be attributed to the simulation of weak wind flow of the model. Overall, HadAM3 performs better than CAM3, and this might be due to an improved physical parameterization scheme in HadAM3 (Pope et al. 2000).

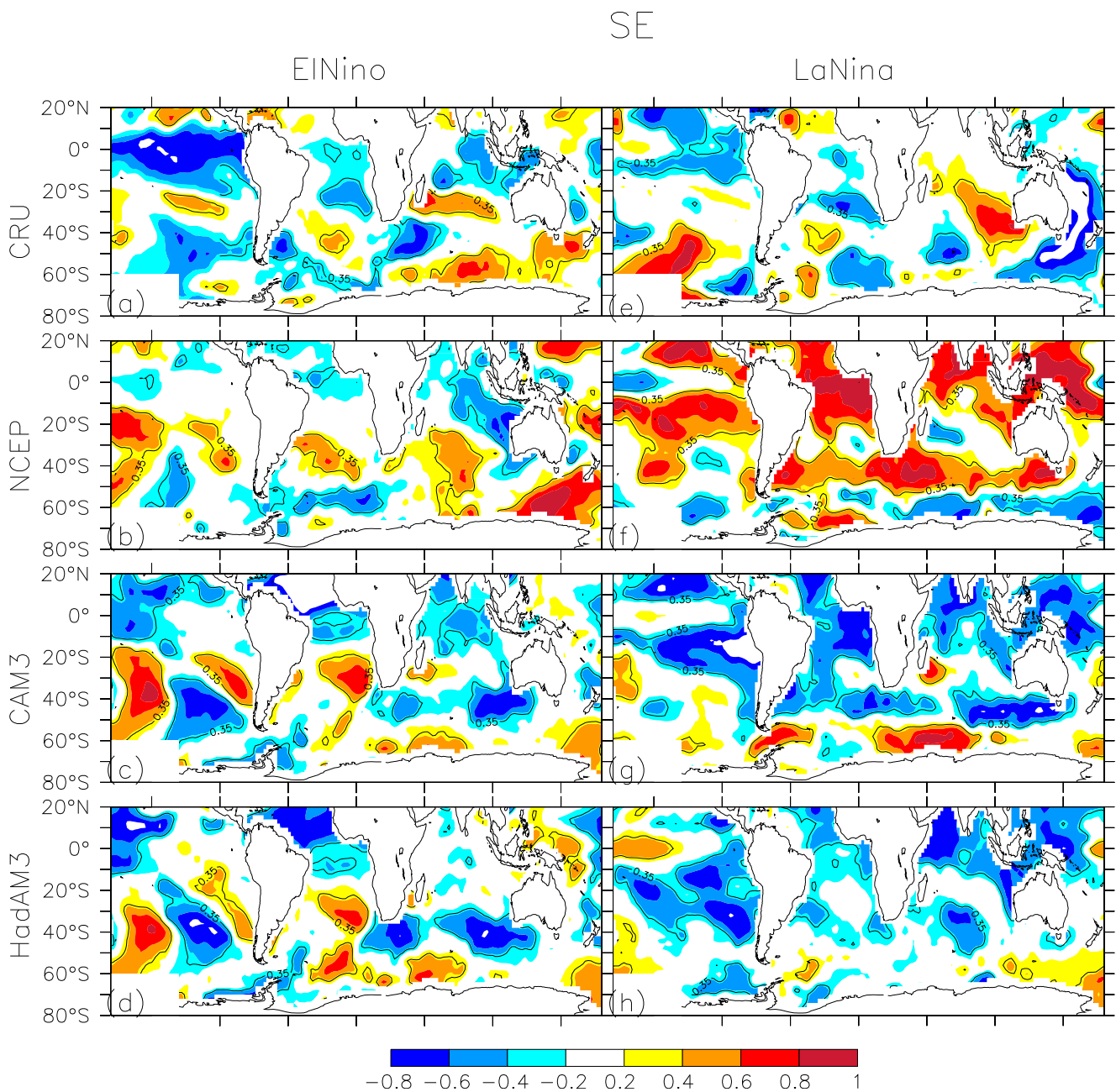


Fig. 18 Same as Fig. 16 but for SE

This study also explored the capability of CAM3 and HadAM3 in representing the time series of rainfall and circulations during ENSO years. It also investigated the relationship between the regional rainfall from the models and global SST during the El Niño and La Niña years. Typical synoptic conditions during the ENSO years appear to be coupled with rainfall variations. For instance, more intense circulation activities advocate strengthening of advection and dry southerly air mass into most parts of the region, which cause the consequential dry rainfall pattern in El Niño years. In La Niña years, more intense conditions prevail, which favor

stronger circulation and tropical convection resulting in above normal rainfall over Southern Africa.

Simulating the influence of SST on the seasonal rainfall over these four regions as observed is challenging for the models, even for the reanalysis. This could be because the models do not fully resolve smaller scale circulations (Gates 1985; Bryan 1984) that control connection between the SST and the seasonal rainfall over Southern Africa. Nonetheless, it is interesting to note that both models give a consistent pattern, which agrees with the observation in some subregions and does not in other subregions. In particular, both models could agree with CRU over NW and SE but not over NE and WC.

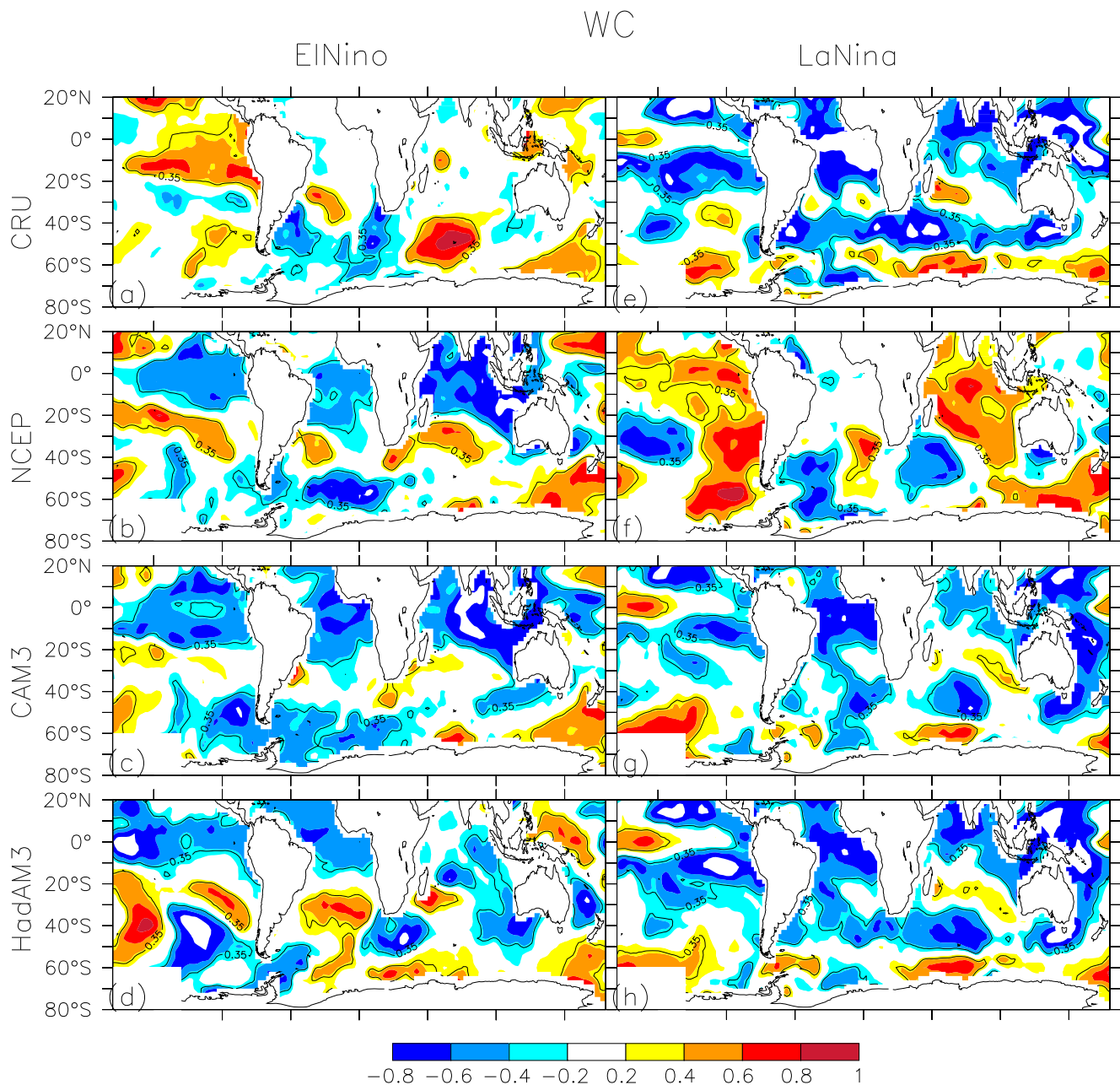


Fig. 19 Distribution of inter-annual temporal correlation coefficients between JJA mean rainfall over the WC subregion and JJA mean global SST for ENSO years from observed, simulated, and reanalysis. Significant values ($r > 0.37$) are in enclosed contours

In summary, although they show some biases, both CAM3 and HadAM3 are able to simulate the essential climatic features and significant relationship between the regional rainfall and SST over the Niño 3.4 region, which strongly drives the climate of Southern Africa. Their simulations could contribute to understanding the climate of the region and improve seasonal forecasts over Southern Africa if models can fully resolve small-scale circulations.

This study has presented an assessment of how well two commonly used GCMs can simulate the climate of

Southern Africa and discussed the usefulness of the models in the multi-model forecasting system over the region. Understanding how well climate models can simulate seasonal climate before adopting them for operational forecast is a very important step which can help to reduce climate risks associated with wrong seasonal forecasts. The information provided in this study is a valuable feedback to modelers and seasonal forecasters on how the models perform over the region. In addition, the study has provided useful metrics for evaluating models for a multi-model seasonal forecasting system.

Acknowledgments The project is sponsored by the Centre for High Performance Computation (CHPC South Africa) and Department of Energy (DOE, USA). The first author is grateful to Schlumberger (faculty for the future fellowship) and DAAD for financial support. The second author is grateful to John Standford for financial support under the incentive project funds at Iowa State University. The authors appreciate the technical support of Climate Systems Analysis Group staff. Lastly, thanks go to the Abdus Salam International Centre for Theoretical Physics, Trieste, Italy, for the opportunity to complete this work.

References

- Bartman AG, Landman WA, Rautenbach CJ, De W (2003) Recalibration of general circulation model output to austral summer rainfall over southern Africa. *Int J Climatol* 23:1407–1419
- Bryan K (1984) Accelerating the convergence to equilibrium of ocean-climate models. *J Phys Oceanogr* 14:666–673
- Collins W, Rasch P, Boville B, Hack J, McCaa J, Williamson D, Kiehl J, Briegleb B, Bitz C, Lin S et al (2004) Description of the NCAR Community Atmosphere Model (CAM 3.0). *NCAR Technical Note*. National Center for Atmospheric Research, Boulder, Colorado. <http://www.cesm.ucar.edu/models/atm-cam>. Accessed 20 Aug 2010
- Cook K (2000) The South Indian convergence zone and inter-annual rainfall variability over southern Africa. *J Clim* 13:3789–3804
- Engelbrecht F, McGregor J, Engelbrecht C (2009) Dynamics of the Conformal-Cubic Atmospheric Model projected climate-change signal over southern Africa. *Int J Climatol* 29(7):1013–1033
- Flocas H, Tolika K, Anagnostopoulou C, Patrikas I, Maheras P, Vafiadis M (2004) Evaluation of maximum and minimum temperature NCEP-NCAR reanalysis data over the Greek area. *Theor Appl Climatol* 80:49–65
- Gates WL (1985) The use of general circulation models in the analysis of the ecosystem impacts of climatic change. *Clim Change* 7:267–284
- Gordon C, Cooper C, Senior C, Banks H, Gregory J, Johns T, Mitchell J, Wood R (2000) The simulation of SST, sea ice extents and ocean heat transports in a version of the Hadley Centre coupled model without flux adjustments. *Clim Dyn* 16(2):147–168
- Gregory D, Allen S (1991) The effect of convective scale downdrafts upon NWP and climate simulations. Preprints. Ninth conference on numerical weather prediction. Amer Meteor Soc, Denver, Colorado, pp 122–123
- Gregory D, Rowntree P (1990) A mass flux convection scheme with representation of cloud ensemble characteristics and stability dependent closure. *Mon Weather Rev* 118(17):1483–1506
- Hack J (1994) Parameterization of moist convection in the National Center for Atmospheric Research community climate model (CCM2). *J Geophys Res* 99(D3):5551–5568
- Halpert MS, Ropelewski CF (1992) Surface temperature patterns associated with the Southern Oscillation. *J Clim* 5:577–593
- Harrison M (1984) The annual rainfall cycle over the central interior of South Africa. *S Afr Geogr J* 66:47–64
- Hines KM, Bromwich DH, Marshall GJ (2000) Artificial surface pressure trends in the NCEP–NCAR reanalysis over the Southern Ocean and Antarctica. *J Clim* 13:3940–3952
- Jones C, Gregory J, Thorpe R, Cox P, Murphy J, Sexton D, Valdes P (2005) Systematic optimisation and climate simulation of FAMOUS, a fast version of HadCM3. *Clim Dyn* 25(2):189–204
- Jury M, Pathack B (1993) Composite climatic patterns associated with extreme modes of summer rainfall over southern Africa: 1975–1984. *Theor Appl Climatol* 47(3):137–145
- Kalnay E, Kanamitsuand M, Kistler R, Collins W, Deaven D, Gandin L, Iredell M, Saha S, White G, Woollen J, Zhu Y, Chelliah M, Ebisuzaki W, Higgins W, Janoia J, Mo KC, Ropelewski C, Wang J, Leetmaa A, Jenne R, Joseph D (1996) The NCEP/NCAR 40-year reanalysis project. *Bull Am Meteorol Soc* 77(2):437–471
- Klaus D (1978) Spatial distribution and periodicity of mean annual precipitation south of the Sahara. *Theor Appl Climatol* 26(1):17–27
- Klopper E, Landman W (2003) A simple approach for combining seasonal forecasts for southern Africa. *Meteorol Appl* 10(4):319–327
- Kraus E (1977) Subtropical droughts and cross-equatorial energy transports. *Mon Weather Rev* 105(8):1009–1018
- Landman W, Goddard L (2002) Statistical recalibration of GCM forecasts over Southern Africa using model output statistics. *J Clim* 15(15):2038–2055
- Landman W, Mason S, Tyson P, Tennant W (2001a) Retro-active skill of multi-tiered forecasts of summer rainfall over southern Africa. *Int J Climatol* 21(1):1–19
- Landman WA, Mason SJ, Tyson PD, Tennant WJ (2001b) Statistical downscaling of GCM simulations to streamflow. *J Hydrol* 252:221–236
- Lin S, Rood R (1996) Multidimensional flux-form semi-Lagrangian transport schemes. *Mon Weather Rev* 124(9):2046–2070
- Mason S, Jury M (1997) Climatic variability and change over southern Africa: a reflection on underlying processes. *Prog Phys Geogr* 21(1):23
- McGregor G, Nieuwolt S (1998) Tropical climatology: an introduction to the climates of the low latitudes, 2nd edn. Wiley, England
- Misra J (1991) Phase synchronization. *Inf Process Lett* 38(2):101–105
- Mitchell TD, Carter TR, Jones PD, Hulme M, New M (2004). A comprehensive set of high-resolution grids of monthly climate for Europe and the globe: the observed record (1901–2000) and 16 scenarios (2001–2100). Tyndall Working Paper 55, Tyndall Centre, UEA, Norwich, UK. <http://www.tyndall.ac.uk/> [Last accessed 19 April 2014]
- Murphy B, Marsiat I, Valdes P (2002). Atmospheric contributions to the surface mass balance of Greenland in the HadAM3 atmospheric model. *J Geophys Res (Atmospheres)*, 107(D21)
- Nakamura H, Shimpo A (2004) Seasonal variations in the Southern Hemisphere storm tracks and jet streams as revealed in a reanalysis dataset. *J Clim* 17:1828–1844
- Newell R, Kidson I (1984) African mean wind changes between Sahelian wet and dry periods. *Int J Climatol* 4:27–33
- Nicholson S (2000) The nature of rainfall variability over Africa on time scales of decades to millenia. *Glob Planet Chang* 26(1–3):137–158
- Nicholson S, Ba M, Kim J (1996) Rainfall in the Sahel during 1994. *J Clim* 9(7):1673–1676
- Ogallal LA (1994). Validity of the ENSO-related impacts in Eastern and Southern Africa, in *Proceedings of the workshop on ENSO/FEWS*, Budapest, Hungary, pp. 179–184
- Philander S (1990) El Niño, La Niña, and the Southern Oscillation. Academic, New York
- Pope V, Gallani M, Rowntree P, Stratton R (2000) The impact of new physical parametrizations in the Hadley Centre climate model: HadAM3. *Clim Dyn* 16(2):146
- Rao VB, Chapa SR, Fernandez JPR, Franchito SH (2002) A diagnosis of rainfall over South America during the 1997/98 El Niño event. Part II: roles of water vapor transport and stationary waves. *J Clim* 15:512–521
- Rasch P, Kristjánsson J (1998) A comparison of the CCM3 model climate using a diagnosed and predicted condensate parameterizations. *J Clim* 11(7):1587–1614
- Rasmusson EM, Wallace JM (1983) Meteorological aspects of the El Niño/Southern Oscillation. *Science* 222:1195–1202
- Reason C (2002) Sensitivity of the southern African circulation to dipole sea-surface temperature patterns in the south Indian Ocean. *Int J Climatol* 22(4):377–393
- Reason C, Jagadheesha D (2005) A model investigation of recent ENSO impacts over southern Africa. *Meteorog Atmos Phys* 89(1):181–205
- Reason CJC, Jagadheesha D, Tadross M (2003) A model investigation of interannual winter rainfall variability over southwestern South

- Africa and associated ocean-atmosphere interaction. *S Afr J Sci* 99: 75–80
- Reynolds R (1988) A real-time global sea surface temperature analysis. *J Clim* 1(1):75–87
- Roca R, Lafore J, Piriou C, Redelsperger J (2005) Extratropical dry-air intrusions into the West African monsoon midtroposphere: an important factor for the convective activity over the Sahel. *J Atmos Sci* 62:390–407
- Rocha A, Simmonds I (1997) Interannual variability of south-eastern African summer rainfall. Part 1: relationships with air-sea interaction processes. *Int J Climatol* 17:235–265. doi:10.1002/(SICI)1097-0088(19970315)
- Ropelewski CF, Halpert MS (1987) Global and regional scale precipitation associated with El Niño/Southern Oscillation. *Mon Weather Rev* 115:985–996
- Rusticucci MM, Kousky VE (2002) A comparative study of maximum and minimum temperatures over Argentina: NCEP-NCAR reanalysis versus station data. *J Clim* 15:2089–2101
- Shongwe ME, Landman WA, Mason SJ (2006) Performance of recalibration systems for GCM forecasts for southern Africa. *Int J Climatol* 17:1567–1585
- Smith SR, Legler DM, Verzone KV (2001) Quantifying uncertainties in NCEP reanalyses using high-quality research vessel observations. *J Clim* 14:4062–4072
- Sundqvist H (1988) Parameterization of condensation and associated clouds in models for weather prediction and general circulation simulation. Physically-based modelling and simulation of climate and climatic change. Springer, New York, pp 433–461
- Suzuki T (2011) Seasonal variation of the ITCZ and its characteristics over central Africa. *Theor App Climatol*, Volume 103, Issue 1-2, pp 39-60
- Taljaard J (1986) Change of rainfall distribution and circulation patterns over Southern Africa in summer. *Int J Climatol* 6(6):579–592
- Taylor KE (2001) Summarizing multiple aspects of model performance in a single diagram. *J Geophys Res* 106:7183–7192
- Thomcroft C, Flocas H (1997) A case study of Saharan cyclogenesis. *Mon Weather Rev* 125:1147–1165
- Tyson P (1980) Temporal and spatial variation of rainfall anomalies in Africa south of latitude 22 during the period of meteorological record. *Clim Chang* 2(4):363–371
- Tyson P (1981) Atmospheric circulation variations and the occurrence of extended wet and dry spells over southern Africa. *Int J Climatol* 1(2)
- Tyson P, Preston-Whyte R (2000) The weather and climate of Southern Africa. Oxford University Press, Southern Africa
- Tyson P, Sturman A, Fitzharris B, Mason S, Owens I (1997) Circulation changes and teleconnections between glacial advances on the west coast of New Zealand and extended spells of drought years in South Africa. *Int J Climatol* 17(14):1499–1512
- Uccellini L, Johnson D (1979) The coupling of upper and lower tropospheric jet streaks and implications for the development of severe convective storms. *Mon Weather Rev* 107(6):682–703
- Usman M, Reason C (2004) Dry spell frequencies and their variability over southern Africa. *Clim Res* 26(3):199–211
- Yang SK, Hou YT, Miller AJ, Campana KA (1999) Evaluation of the Earth radiation budget in NCEP-NCAR reanalysis with ERBE. *J Clim* 12:477–493
- Zhang G, McFarlane N (1995) Sensitivity of climate simulations to the parameterization of cumulus convection in the Canadian Climate Centre general circulation model. *Atmos Ocean* 33:407
- Zhang F, Snyder C, Rotunno R (2003) Effects of moist convection on mesoscale predictability. *J Atmos Sci* 60(9):1173–1185